The Astrophysical Journal Supplement Series, 140:589–607, 2002 June

LABORATORY MEASUREMENTS AND IDENTIFICATION OF THE Fe XVIII–XXIV L-SHELL X-RAY LINE EMISSION

G. V. Brown,[1] P. Beiersdorfer, D. A. Liedahl, and K. Widmann
Department of Physics and Advanced Technology, Lawrence Livermore National Laboratory, 7000 East Avenue, Livermore, CA 94551

S. M. Kahn
Department of Physics and Columbia Astrophysics Laboratory, Columbia University, New York, NY 10027

and

E. J. Clothiaux
Department of Physics, Auburn University, Auburn, AL 36849
Received 2001 November 1; accepted 2001 December 28

ABSTRACT

A comprehensive survey of $\Delta n \geq 1$ iron L-shell X-ray line emission is presented. We have used the electron beam ion trap EBIT-II at the Lawrence Livermore National Laboratory and equipped with flat crystal spectrometers to measure the wavelengths of over 150 features between 10.6 and 18 Å. We present wavelengths, line identifications, and relative intensities of all of the significant $\Delta n \geq 1$ L-shell line emission from Fe XVIII–XXIV at electron densities of $\sim 10^{12}$ cm^{-3} resulting from direct electron impact excitation from the ground state followed by radiative cascades. This data set includes 2–3 times as many lines as are found in current standard line lists.

Subject headings: atomic data — line: identification — stars: coronae — Sun: corona — Sun: X-rays, gamma rays — X-rays: general

1. INTRODUCTION

The arrival of the first high spectral resolution data sets from the *Chandra X-Ray Observatory* (*CXO*) (Brinkman et al. 2000; Canizares et al. 2000) and the *X-ray Multi-Mirror Mission* (*XMM*) (Audard et al. 2001a; Audard, Güdel, & Mewe 2001b; Kahn et al. 2001) have established a new era in X-ray astrophysics. The launch of *Astro-E2* in 2005 will complete the triad of X-ray observatories. The spectra obtained by these missions provide detailed constraints on the complex physical processes occurring in hot cosmic plasmas and make possible X-ray line diagnostics for a wide range of astrophysical sources. Accurate interpretation of these data relies heavily on the accuracy of the atomic data on which the line diagnostics are based. However, the level of accuracy and completeness of these databases, although provided by laboratory and solar experiments of high accuracy and augmented by reliable atomic calculations, in many cases falls short of what is required for full exploitation of the spectra these missions provide.

An indication of the inadequacy of available atomic databases came with some of the attempts to fit much lower resolution spectra acquired by the *Advanced Satellite for Cosmology and Astrophysics* (*ASCA*) (Brickhouse et al. 2000, 1997; Fabian et al. 1994). In many cases, systematic discrepancies between the data and the best fitting models were found in the 6–18 Å wavelength region. Part of this problem was attributed to the quality and quantity of the atomic data on which the fitting packages are based (White 1996; Liedahl et al. 1995; Fabian et al. 1994). Subsequent laboratory measurements have indeed shown that line intensities are modeled incorrectly (Gu et al. 1999; Savin et al. 1996) and that many lines are not present in the available spectral synthesis codes (Brown et al. 1998).

CXO, *XMM-Newton*, and *Astro-E2* provide spectra in the 10–18 Å wavelength range with resolving power 1–2 orders of magnitude higher than *ASCA*, i.e., on a level comparable to or better than solar spectra (McKenzie et al. 1980; Phillips et al. 1982). These data mandate a much higher level of accuracy and completeness for spectral fitting packages if they are to provide a reliable platform for interpretation.

Examples of the effect that better atomic data have on the modeling of high-resolution spectra in the 5–23 Å region has been demonstrated in the analysis of solar and nonsolar spectra. In the case of solar spectra, Phillips et al. (1999) have compared the wavelengths previously used in the MEKAL model with better and newer measurements by the flat crystal spectrometer (FCS) on board the *Solar Maximum Mission* (*SMM*), measured spectra from the Princeton Large Torus (PLT) tokamak (Wargelin et al. 1998), and some of the preliminary results from the EBIT-II electron beam ion trap measurements we present in this paper. By shifting the MEKAL wavelengths to more reliable measured values they achieved a factor of 2 improvement in χ^2 when fitting *SMM* spectral data. Once the wavelengths were adjusted, extra flux was added in the form of several Gaussian lines to account for emission lines observed in the solar spectra but missing from MEKAL. This addition reduced their χ^2 by another 30%. Improvement beyond that attained by the addition of more accurate wavelengths and the inclusion of more lines can be expected once better models for the line emissivities are added (Gu et al. 1999; Liedahl, Osterheld, & Goldstein 1995).

In the case of recent nonsolar spectra, Behar, Cottam, & Kahn (2001) have analyzed the publicly available high-resolution spectra of Capella obtained by the High Energy Transmission Grating on the *CXO*. They showed that only

[1] Currently at NASA Goddard Space Flight Center, Greenbelt, MD 20770; gvb@milkyway.gsfc.nasa.gov.

TABLE 1
BEAM ENERGIES AND IONIZATION ENERGIES OF EACH CHARGE STATE MEASURED

Charge State	Acq. Energy (keV)	Ion. Energy (keV)	Spectral Positions	Concatenation Wavelengths
Fe XVIII	1.34 ± 0.03	1.36	6	11.68, 12.61, 13.91, 14.95, 16.20
Fe XIX.....	1.44 ± 0.03	1.46	5	12.60, 13.90, 14.80, 16.20
Fe XX.....	1.55 ± 0.03	1.58	4	11.47, 12.67, 13.91
Fe XXI.....	1.66 ± 0.03	1.69	3	12.67, 13.87
Fe XXII.....	1.76 ± 0.03	1.80	3	11.60, 12.70
Fe XXIII	1.88 ± 0.03	1.95	2	11.60
Fe XXIV.....	2.05 ± 0.03	2.05	2	11.60
Fe XXIV.....	4.6 ± 0.1	2.05	1	...

by using accurate wavelengths from laboratory measurements, i.e., the laboratory values presented here, and a full calculation of the line intensities was it possible to fit high-resolution Capella spectra correctly.

In this paper, we present the results of an extensive series of measurements undertaken at the electron beam ion trap EBIT-II located at the Lawrence Livermore National Laboratory (LLNL), of line emission from Fe XVIII–XXIV in the 10–18 Å spectral region. The results include wavelengths, line identifications, and relative intensities of 155 features. In an earlier paper (Brown et al. 1998), we provided similar measurements for the specific case of Fe XVII.

2. EXPERIMENTAL SETUP

These measurements were conducted using flat crystal spectrometers on the EBIT-II electron beam ion trap. EBIT-II is a well characterized source which has been described elsewhere (Beiersdorfer et al. 2000a; Marrs 1995; Marrs, Beiersdorfer, & Schneider 1994; Levine et al. 1988) and extensively utilized for wavelength measurements and laboratory astrophysics (Brown et al. 2001; Beiersdorfer et al. 2000b; Porter et al. 2000; Lepson et al. 2000). In brief, EBIT-II consists of an electron beam, an electrostatic trapping region in which ion-electron interactions take place, a collector where the beam is collected, and a metal vacuum vapor arc (MeVVA) used for the injection of the target ions. The MeVVA produces singly or doubly ionized ions which are trapped and further ionized to the desired charge state collisionally by the electron beam. The flat crystal spectrometers used for these measurements employ either a thallium acid phthalate (TlAP), cesium acid phthalate (CsAP) (each $50 \times 25 \times 2$ mm), or rubidium acid phthalate (RAP) crystal (250 mm $\times$ 12.5 mm $\times$ 2 mm) for dispersion, and a gas-filled, position-sensitive proportional counter (PSPC) for detection. The spectrometer operates at a pressure of $\approx 10^{-3}$ Pa in order to avoid the absorption of X-rays by air. The vacuum of EBIT-II is less than 10^{-8} Pa; consequently, it is necessary to provide a barrier between the spectrometer and EBIT-II to preserve the integrity of EBIT-II's vacuum. This barrier is provided by a 25 mm diameter $\times$ 1.0 μm thick polyimide window. In addition to this window, the PSPC employs a 4 μm thick polypropylene window coated with 200–400 Å of aluminum to isolate its detection chamber ($P = 1.0 \times 10^5$ Pa of P-10 gas) from the chamber of the spectrometer. A description of the instrumentation is given by Beiersdorfer & Wargelin (1994) and by Brown, Beiersdorfer, & Widmann (1999).

Owing to the large range of ionization stages measured, several different beam energies were required to complete this line survey (see Table 1). Generally, the beam energy was set just slightly below the ionization energy of the desired charge state so as to populate the greatest number of high-n levels. Because of the size of the crystals used, more than one crystal position was required to cover the 10.6–18.0 Å spectral range presented here. Furthermore, because the wavelength band spanned by the emission from each charge state varies, the number of spectra required for each

TABLE 2
COMPARISON OF MEASUREMENTS AND CALCULATIONS OF Fe XVIII LINES

	HULLAC						THIS MEASUREMENT		PHILLIPS[a]	MEKA[b]	KELLY 1987	
LABEL	Upper	J'	Lower	J	λ (Å)	I	λ (Å)	I[c]	λ (Å)	λ (Å)	λ (Å)	References
F1[d].....	$1s^2 2s^2 2p_{1/2} 2p_{3/2}^3 3p_{1/2}$	$\frac{3}{2}$	$1s^2 2s_{1/2} 2p^2 2p^4$	$\frac{1}{2}$	17.664	0.4	17.623 (3)	0.5	17.626	...	...	...
F2	$1s^2 2s_{1/2} 2p^2 2p_{3/2}^3 3s$	$\frac{3}{2}$	$1s^2 2s_{1/2} 2p^2 2p^4$	$\frac{1}{2}$	16.345	< 0.1	16.320 (5)	0.2	16.310	16.310	...	...
F3	$1s^2 2s_{1/2} 2p_{1/2} 2p^4 3s$	$\frac{3}{2}$	$1s^2 2s_{1/2} 2p^2 2p^4$	$\frac{1}{2}$	16.197	0.2	16.159 (5)	0.2	16.165	16.170	16.166	1
F4	$1s^2 2s^2 2p^2 2p_{3/2}^2 3s$	$\frac{5}{2}$	$1s^2 2s^2 2p^2 2p_{3/2}^3$	$\frac{3}{2}$	16.097	0.5	16.071 (3)	0.9	16.078	16.074	16.073	2
F5	$1s^2 2s^2 2p_{1/2} 2p_{3/2}^3 3s$	$\frac{1}{2}$	$1s^2 2s^2 2p_{1/2} 2p^4$	$\frac{1}{2}$	16.044	< 0.1	16.045 (10)	0.3	16.018	16.020	16.024	2
F6	$1s^2 2s^2 2p^2 2p_{3/2}^2 3s$	$\frac{3}{2}$	$1s^2 2s^2 2p^2 2p_{3/2}^3$	$\frac{3}{2}$	16.023	0.4	16.004 (2)	0.6	16.002	...	16.003	2
F7	$1s^2 2s^2 2p^2 2p_{3/2}^2 3s$	$\frac{1}{2}$	$1s^2 2s^2 2p^2 2p_{3/2}^3$	$\frac{3}{2}$	15.901	< 0.1	15.931 (8)	0.1	15.901	...	...	...
F8	$1s^2 2s^2 2p_{1/2} 2p_{3/2}^3 3s$	$\frac{3}{2}$	$1s^2 2s^2 2p_{1/2} 2p^4$	$\frac{1}{2}$	15.883	0.1	15.870 (3)	0.3	15.874	15.868	15.869	2
F9	$1s^2 2s^2 2p_{1/2} 2p_{3/2}^3 3s$	$\frac{3}{2}$	$1s^2 2s^2 2p^2 2p_{3/2}^3$	$\frac{3}{2}$	15.853	0.2	15.824 (3)	0.2	15.831	15.828	15.826	2

TABLE 2—*Continued*

	HULLAC						This Measurement		Phillips[a]	MEKA[b]	Kelly 1987	
Label	Upper	J'	Lower	J	λ (Å)	I	λ (Å)	I[c]	λ (Å)	λ (Å)	λ (Å)	References
F10	$1s^2 2s^2 2p_{1/2} 2p_{3/2}^3 3s$	$\frac{1}{2}$	$1s^2 2s^2 2p^2 2p_{3/2}^3$	$\frac{3}{2}$	15.787	< 0.1	15.759 (5)	0.1	15.765	15.769	15.764	2
F11	$1s^2 2s^2 2p_{1/2} 2p_{3/2}^3 3s$	$\frac{5}{2}$	$1s^2 2s^2 2p^2 2p_{3/2}^3$	$\frac{3}{2}$	15.641	0.4	15.625 (3)	0.4	15.628	15.632	15.623	2, 3
F12	$1s^2 2s_{1/2} 2p^2 2p_{3/2}^3 3s$	$\frac{3}{2}$	$1s^2 2s_{1/2} 2p^2 2p^4$	$\frac{1}{2}$	15.501	< 0.1	15.494 (10)	0.1	15.498	15.496[e]	...	...
F13	$1s^2 2s^2 2p^2 2p_{3/2}^2 3d_{5/2}$	$\frac{1}{2}$	$1s^2 2s^2 2p^2 2p_{3/2}^3$	$\frac{3}{2}$	14.601	< 0.1	14.616 (10)	0.1	14.588	14.611	14.610	1
F14	$1s^2 2s^2 2p^2 2p_{3/2}^2 3d_{5/2}$	$\frac{3}{2}$	$1s^2 2s^2 2p^2 2p_{3/2}^3$	$\frac{3}{2}$	14.568	0.1	14.571 (11)	<0.1	14.555	14.553	14.551	2
F15	$1s^2 2s^2 2p^2 2p_{3/2}^2 3d_{5/2}$	$\frac{5}{2}$	$1s^2 2s^2 2p^2 2p_{3/2}^3$	$\frac{3}{2}$	14.548	0.3	14.534 (3)	0.3	14.540	...	14.536	2
F16	$1s^2 2s^2 2p_{1/2} 2p_{3/2}^3 3d_{5/2}$	$\frac{3}{2}$	$1s^2 2s^2 2p_{1/2} 2p^4$	$\frac{1}{2}$	14.424	< 0.1	14.425 (9)	0.1	14.422	14.426	...	...
F17	$1s^2 2s^2 2p_{1/2} 2p_{3/2}^3 3d_{3/2}$	$\frac{5}{2}$	$1s^2 2s^2 2p^2 2p_{3/2}^3$	$\frac{3}{2}$	14.386	0.4	14.373 (6)	0.4	14.378	14.374	14.373	2
F18	$1s^2 2s^2 2p_{1/2} 2p_{3/2}^3 3d_{3/2}$	$\frac{1}{2}$	$1s^2 2s^2 2p_{1/2} 2p^4$	$\frac{1}{2}$	14.360	0.1	14.343 (10)	0.1	14.360	14.360	14.344	1
F19	$1s^2 2s^2 2p_{1/2} 2p_{3/2}^3 3d_{3/2}$	$\frac{1}{2}$	$1s^2 2s^2 2p^2 2p_{3/2}^3$	$\frac{3}{2}$	14.276	0.2	14.256(5)	0.1	14.260	...	...	...
	$1s^2 2s^2 2p_{1/2} 2p_{3/2}^3 3d_{5/2}$	$\frac{5}{2}$	$1s^2 2s^2 2p^2 2p_{3/2}^3$	$\frac{3}{2}$	14.267	< 0.1			14.267	14.281	...	...
F20	$1s^2 2s^2 2p_{1/2} 2p_{3/2}^3 3d_{5/2}$	$\frac{3}{2}$	$1s^2 2s^2 2p^2 2p_{3/2}^3$	$\frac{3}{2}$	14.216	0.5	14.208 (3)	1	14.212	14.220[f]	...	...
	$1s^2 2s^2 2p_{1/2} 2p_{3/2}^3 3d_{3/2}$	$\frac{5}{2}$	$1s^2 2s^2 2p^2 2p_{3/2}^3$	$\frac{3}{2}$	14.203	1.0			14.204	...	14.202	2
F21	$1s^2 2s^2 2p_{1/2} 2p_{3/2}^3 3d_{3/2}$	$\frac{3}{2}$	$1s^2 2s^2 2p^2 2p_{3/2}^3$	$\frac{3}{2}$	14.154	< 0.1	14.158 (15)	<0.1	14.154	14.152	14.150	2
F22	$1s^2 2s^2 2p_{3/2}^4 3d_{5/2}$	$\frac{5}{2}$	$1s^2 2s^2 2p^2 2p_{3/2}^3$	$\frac{3}{2}$	13.979	< 0.1	13.953 (11)	0.1	13.960	13.957	13.954	2
F23	$1s^2 2s_{1/2} 2p^2 2p_{3/2}^3 3p_{1/2}$	$\frac{5}{2}$	$1s^2 2s^2 2p^2 2p_{3/2}^3$	$\frac{3}{2}$	13.464	< 0.1	13.451 (8)	<0.1	13.453	...	13.464	1
F24	$1s^2 2s_{1/2} 2p^2 2p_{3/2}^3 3p_{3/2}$	$\frac{3}{2}$	$1s^2 2s^2 2p^2 2p_{3/2}^3$	$\frac{3}{2}$	13.419	< 0.1	13.407 (4)	<0.1	13.406	...	...	...
F25	$1s^2 2s_{1/2} 2p_{1/2} 2p^4 3p_{1/2}$	$\frac{3}{2}$	$1s^2 2s^2 2p^2 2p_{3/2}^3$	$\frac{3}{2}$	13.347	< 0.1	13.355 (9)	<0.1	13.357	13.354	13.355	1
F26	$1s^2 2s_{1/2} 2p_{1/2} 2p^4 3p_{1/2}$	$\frac{1}{2}$	$1s^2 2s^2 2p^2 2p_{3/2}^3$	$\frac{3}{2}$	13.315	< 0.1	13.323 (5)	<0.1	13.323	13.329	...	...
	$1s^2 2s_{1/2} 2p^2 2p_{3/2}^3 3p_{3/2}$	$\frac{5}{2}$	$1s^2 2s^2 2p^2 2p_{3/2}^3$	$\frac{3}{2}$	13.312	< 0.1			13.312	...	13.319	1
F27	$1s^2 2s_{1/2} 2p_{1/2} 2p^4 3p_{3/2}$	$\frac{5}{2}$	$1s^2 2s^2 2p^2 2p_{3/2}^3$	$\frac{3}{2}$	12.819	< 0.1	12.843 (7)	<0.1	12.838	...	12.847	1
F28	$1s^2 2s^2 2p^2 2p_{3/2}^2 4s$	$\frac{3}{2}$	$1s^2 2s^2 2p^2 2p_{3/2}^3$	$\frac{3}{2}$	11.878	< 0.1	11.861 (12)	<0.1	11.864	...	...	...
F29	$1s^2 2s_{1/2} 2p^2 2p_{3/2}^3 4d_{5/2}$	$\frac{3}{2}$	$1s^2 2s_{1/2} 2p^2 2p^4$	$\frac{1}{2}$	11.744	< 0.1	11.75–11.68	<0.1	11.739	...	...	...
	$1s^2 2s_{1/2} 2p^2 2p_{3/2}^3 4d_{5/2}$	$\frac{1}{2}$	$1s^2 2s_{1/2} 2p^2 2p^4$	$\frac{1}{2}$	11.724	< 0.1			...	...	...	...
	$1s^2 2s^2 2p^2 2p_{3/2}^2 4d_{5/2}$	$\frac{1}{2}$	$1s^2 2s^2 2p_{1/2} 2p^4$	$\frac{1}{2}$	11.689	< 0.1			...	...	...	...
	$1s^2 2s_{1/2} 2p^2 2p_{3/2}^3 4d_{3/2}$	$\frac{3}{2}$	$1s^2 2s_{1/2} 2p_{1/2}^2 2p^4$	$\frac{1}{2}$	11.682	< 0.1			...	...	...	...
F30	$1s^2 2s^2 2p^2 2p_{3/2}^2 4d_{5/2}$	$\frac{3}{2}$	$1s^2 2s^2 2p_{1/2} 2p^4$	$\frac{1}{2}$	11.675	< 0.1	11.642 (7)	<0.1	...	...	...	...
F31	$1s^2 2s^2 2p_{1/2} 2p_{3/2}^3 4d_{5/2}$	$\frac{3}{2}$	$1s^2 2s^2 2p_{1/2} 2p^4$	$\frac{1}{2}$	11.562	< 0.1	11.574 (6)	<0.1	...	...	11.575	1
	$1s^2 2s^2 2p^2 2p_{3/2}^2 4d_{5/2}$	$\frac{1}{2}$	$1s^2 2s^2 2p^2 2p_{3/2}^3$	$\frac{3}{2}$	11.552	< 0.1	11.574 (6)	<0.1	11.546	...	11.551	1
F32	$1s^2 2s^2 2p^2 2p_{3/2}^2 4d_{5/2}$	$\frac{3}{2}$	$1s^2 2s^2 2p^2 2p_{3/2}^3$	$\frac{3}{2}$	11.539	< 0.1	11.527 (4)	0.1	11.530	11.535	...	...
	$1s^2 2s^2 2p^2 2p_{3/2}^2 4d_{5/2}$	$\frac{5}{2}$	$1s^2 2s^2 2p^2 2p_{3/2}^3$	$\frac{3}{2}$	11.535	0.1	11.527 (4)	0.1	11.526	11.535	11.526	1
F33	$1s^2 2s^2 2p^2 2p_{3/2}^2 4d_{3/2}$	$\frac{3}{2}$	$1s^2 2s^2 2p^2 2p_{3/2}^3$	$\frac{3}{2}$	11.474	< 0.1	11.48–11.43	<0.1	...	...	...	...
	$1s^2 2s^2 2p_{1/2} 2p_{3/2}^3 4d_{3/2}$	$\frac{1}{2}$	$1s^2 2s^2 2p_{1/2} 2p^4$	$\frac{1}{2}$	11.472	< 0.1			...	...	...	...
	$1s^2 2s^2 2p^2 2p_{3/2}^2 4d_{5/2}$	$\frac{5}{2}$	$1s^2 2s^2 2p^2 2p_{3/2}^3$	$\frac{3}{2}$	11.471	< 0.1			...	...	...	...
	$1s^2 2s^2 2p_{1/2} 2p_{3/2}^3 4d_{3/2}$	$\frac{3}{2}$	$1s^2 2s^2 2p_{1/2} 2p^4$	$\frac{1}{2}$	11.467	< 0.1			11.460	11.451	...	...
	$1s^2 2s^2 2p_{1/2} 2p_{3/2}^3 4d_{3/2}$	$\frac{3}{2}$	$1s^2 2s^2 2p^2 2p_{3/2}^3$	$\frac{3}{2}$	11.452	< 0.1			...	11.467	...	...
	$1s^2 2s^2 2p_{1/2} 2p_{3/2}^3 4d_{3/2}$	$\frac{3}{2}$	$1s^2 2s^2 2p_{1/2} 2p^4$	$\frac{1}{2}$	11.448	< 0.1			...	...	...	...
	$1s^2 2s^2 2p_{1/2} 2p_{3/2}^3 4d_{5/2}$	$\frac{5}{2}$	$1s^2 2s^2 2p^2 2p_{3/2}^3$	$\frac{3}{2}$	11.446	< 0.1			...	...	...	...
	$1s^2 2s^2 2p_{1/2} 2p_{3/2}^3 4d_{5/2}$	$\frac{1}{2}$	$1s^2 2s^2 2p_{1/2} 2p^4$	$\frac{1}{2}$	11.444	< 0.1			11.444	...	...	...
F34	$1s^2 2s^2 2p_{1/2} 2p_{3/2}^3 4d_{3/2}$	$\frac{5}{2}$	$1s^2 2s^2 2p^2 2p_{3/2}^3$	$\frac{3}{2}$	11.433	0.1	11.423 (4)	<0.1	11.421	11.430	11.420	1
F35	$1s^2 2s^2 2p_{1/2} 2p_{3/2}^3 4d_{3/2}$	$\frac{1}{2}$	$1s^2 2s^2 2p^2 2p_{3/2}^3$	$\frac{3}{2}$	11.340	< 0.1	11.326 (4)	0.1	11.326	...	...	...
	$1s^2 2s^2 2p_{1/2} 2p_{3/2}^3 4d_{5/2}$	$\frac{3}{2}$	$1s^2 2s^2 2p^2 2p_{3/2}^3$	$\frac{3}{2}$	11.335	< 0.1	11.326 (4)	0.1	11.326	11.336	11.326	1
	$1s^2 2s^2 2p_{1/2} 2p_{3/2}^3 4d_{3/2}$	$\frac{5}{2}$	$1s^2 2s^2 2p^2 2p_{3/2}^3$	$\frac{3}{2}$	11.330	< 0.1	11.326 (4)	0.1	11.326	...	...	...
F36	$1s^2 2s^2 2p_{1/2} 2p_{3/2}^3 4d_{3/2}$	$\frac{3}{2}$	$1s^2 2s^2 2p^2 2p_{3/2}^3$	$\frac{3}{2}$	11.317	< 0.1	11.293 (7)	< 0.1	...	...	...	...

[a] Phillips et al. 1999.
[b] Mewe et al. 1985.
[c] See § 3 for explanation of relative intensity.
[d] This identification was first given in Drake et al. (1999).
[e] Nearest line given by MEKA has $J = 1/2$ upper level.
[f] Nearest line given by MEKA has $J = 5/2$ upper level.

References.—References from Kelly 1987 compilation: (1) Bromage et al. 1977; (2) Feldman et al. 1973; (3) Boiko et al. 1978.

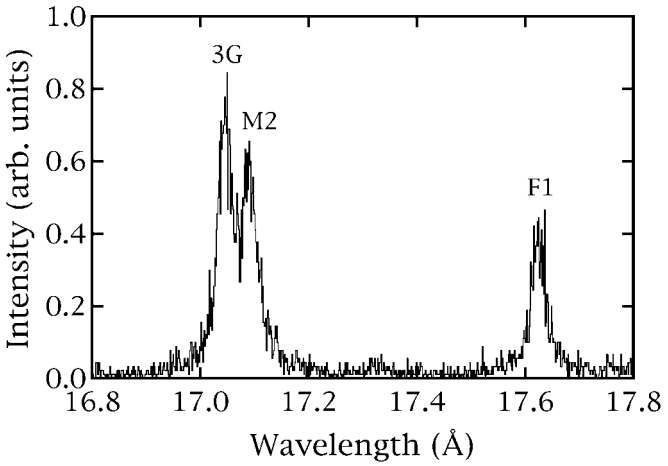

FIG. 1*a*

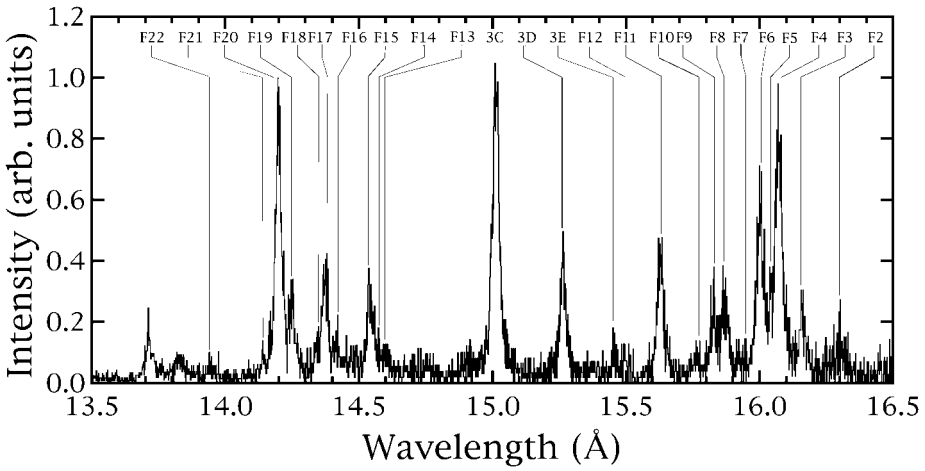

FIG. 1*b*

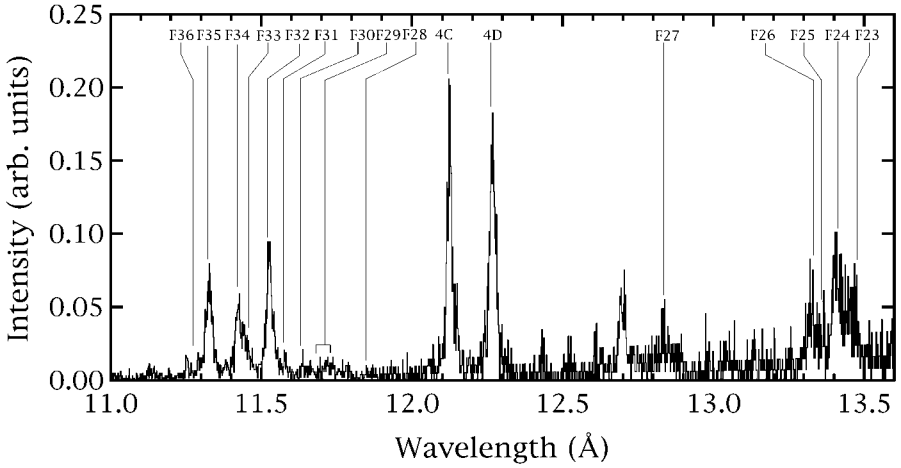

FIG. 1*c*

FIG. 1.—(*a*) Fe XVIII spectrum between 16.8 and 17.9 Å normalized to F20. The lines labeled 3G and M2 are Fe XVII. A detailed discussion of F1 is given by Drake et al. (1999). (*b*) Fe XVIII spectrum between 13.5 and 16.5 Å normalized to F20. This spectrum still includes the stronger Fe XVII lines 3C, 3D, and 3E. (*c*) Fe XVIII spectrum between 11 and 13.6 Å normalized to F20. The lines labeled 4C and 4D are Fe XVII. The scale is ~20% of the scale of (*b*).

charge state also varies. Table 1 shows the number of spectral positions required for each charge state and gives the concatenation wavelength, i.e., the wavelength that the spectra from each crystal position are joined to create the spectra given in Figures 1–7. This procedure is the same as the one followed by Brown et al. (1998) and Beiersdorfer & Wargelin (1994) in the measurement of the Fe XVII data.

TABLE 3

COMPARISON OF MEASUREMENTS AND CALCULATIONS OF Fe XIX LINES

	HULLAC						THIS MEASUREMENT		PHILLIPS[a]	MEKA[b]	KELLY 1987	
LABEL	Upper	J'	Lower	J	λ (Å)	I	λ (Å)	I[c]	λ (Å)	λ (Å)	λ (Å)	Reference
O1	$1s^22s^22p_{1/2}2p_{3/2}^2 3p_{1/2}$	2	$1s^22s_{1/2}2p_{3/2}2p^4$	1	16.286	0.1	16.283 (16)	0.5	16.282	...	...	...
O2	$1s^22s^22p_{1/2}2p_{3/2}^2 3p_{1/2}$	2	$1s^22s_{1/2}2p^22p_{3/2}^3$	2	16.124	0.5	16.110 (4)	0.8	16.106	...	...	...
O3	$1s^22s^22p_{1/2}2p_{3/2}^2 3p_{1/2}$	0	$1s^22s_{1/2}2p_{3/2}2p^4$	1	16.083	<0.1	16.027 (7)	0.3	...	...	...	...
O4	$1s^22s_{1/2}2p_{1/2}2p_{3/2}^3 3s_{1/2}$	2	$1s^22s_{1/2}2p^22p_{3/2}^3$	1	15.412	<0.1	15.40–15.30	0.4	...	...	15.413	1, 2
	$1s^22s_{1/2}2p^22p_{3/2}^2 3s_{1/2}$	2	$1s^22s_{1/2}2p_{1/2}2p^4$	1	15.364	0.1			15.364	...	...	...
	$1s^22s_{1/2}2p^22p_{3/2}^2 3s_{1/2}$	2	$1s^22s_{1/2}2p^22p_{3/2}^3$	2	15.350	0.1			15.358	...	...	
	$1s^22s^22p^22p_{3/2}3s_{1/2}$	2	$1s^22s^22p_{1/2}2p_{3/2}^3$	1	15.308	<0.1			...	...		...
O5	$1s^22s_{1/2}2p^22p_{3/2}^2 3s_{1/2}$	2	$1s^22s_{1/2}2p_{3/2}^2 2p^3$	2	15.220	0.3	15.198 (5)	0.3	15.210	...	15.193	2, 3
O6	$1s^22s^22p^22p_{3/2}3s_{1/2}$	1	$1s^22s^22p_{1/2}2p_{3/2}^3$	1	15.182	<0.1	15.177 (8)	0.2	...	...	15.172	3
O6	$1s^22s_{1/2}2p_{1/2}2p_{3/2}^3 3s_{1/2}$	0	$1s^22s_{1/2}2p_{3/2}2p^4$	1	15.197	<0.1	15.177 (8)	0.2	...	...		
O7	$1s^22s^22p^22p_{3/2}3s_{1/2}$	1	$1s^22s^22p^22p_{3/2}^2$	0	15.151	<0.1	15.134 (5)	0.2	...	...	15.138	3
O8	$1s^22s^22p^22p_{3/2}3s_{1/2}$	2	$1s^22s^22p^22p_{3/2}^2$	2	15.109	0.4	15.079 (4)	0.9	15.114	...	15.111	3
O9	$1s^22s^22p^22p_{3/2}3s_{1/2}$	1	$1s^22s^22p^22p_{3/2}^2$	2	14.985	0.2	14.980 (5)	0.5	14.980	14.962	14.966	3
O10	$1s^22s^22p_{1/2}2p_{3/2}^2 3s_{1/2}$	1	$1s^22s^22p_{1/2}2p_{3/2}^3$	1	14.943	<0.1	14.917 (9)	0.2	14.931	...	...	...
	$1s^22s^22p_{1/2}2p_{3/2}^2 3s_{1/2}$	2	$1s^22s^22p_{1/2}2p_{3/2}^3$	1	14.948	<0.1			...	14.919	14.929	3
O11	$1s^22s_{1/2}2p_{1/2}2p_{3/2}^3 3s_{1/2}$	2	$1s^22s_{1/2}2p_{3/2}2p^4$	1	14.877	<0.1	14.868 (9)	0.1	...	...	...	...
O12	$1s^22s^22p_{1/2}2p_{3/2}^2 3s_{1/2}$	2	$1s^22s^22p^22p_{3/2}^2$	2	14.757	0.1	14.725 (7)	0.2	14.750	14.743	14.735	
O13	$1s^22s^22p_{1/2}2p_{3/2}^2 3s_{1/2}$	3	$1s^22s^22p^22p_{3/2}^2$	2	14.680	0.3	14.664 (7)	0.5	14.670	14.671	14.668	3
O14	$1s^22s_{1/2}2p^22p_{3/2}^2 3d_{3/2}$	3	$1s^22s_{1/2}2p^22p_{3/2}^3$	2	14.093	<0.1	14.127 (10)	0.1	...	...	...	...
	$1s^22s_{1/2}2p_{1/2}2p_{3/2}^3 3d_{3/2}$	3	$1s^22s_{1/2}2p^22p_{3/2}^3$	2	14.071	0.1			...	...	...	...
	$1s^22s_{1/2}2p^22p_{3/2}^2 3d_{5/2}$	1	$1s^22s_{1/2}2p^22p_{3/2}^3$	2	14.055	0.1			...	...	...	...
	$1s^22s_{1/2}2p^22p_{3/2}^2 3d_{5/2}$	2	$1s^22s_{1/2}2p^22p_{3/2}^3$	2	14.049	<0.1			...	...	...	...
	$1s^22s_{1/2}2p_{3/2}^4 3d_{3/2}$	2	$1s^22s_{1/2}2p_{1/2}2p_{3/2}^4$	1	14.039	<0.1			...	...	...	...
O15	$1s^22s^22p^22p_{3/2}3d_{5/2}$	2	$1s^22s^22p_{1/2}2p_{3/2}^3$	1	14.027	<0.1	14.034 (8)	0.2	14.018	14.020	14.021	3
O16	$1s^22s_{1/2}2p^22p_{3/2}^2 3d_{5/2}$	3	$1s^22s_{1/2}2p^22p_{3/2}^3$	2	13.956	<0.1	13.956 (8)	0.1	...	...	13.936	3
O17	$1s^22s^22p^22p_{3/2}3d_{3/2}$	2	$1s^22s^22p^22p_{3/2}^2$	2	13.954	0.1	13.934 (8)	0.3	13.935	...	...	...
	$1s^22s^22p^22p_{3/2}3d_{3/2}$	3	$1s^22s^22p^22p_{3/2}^2$	2	13.954	0.1			13.935			
	$1s^22s^22p_{1/2}2p_{3/2}^2 3d_{3/2}$	1	$1s^22s^22p^22p_{3/2}^2$	2	13.954	<0.1			13.935			
	$1s^22s^22p_{1/2}2p_{3/2}^2 3d_{5/2}$	1	$1s^22s^22p^22p_{3/2}^2$	0	13.952	<0.1			...	...	...	
O18	$1s^22s^22p^22p_{3/2}3d_{5/2}$	1	$1s^22s^22p_{1/2}2p_{3/2}^3$	2	13.875	<0.1	13.839 (5)	0.2	...	...	...	...
	$1s^22s^22p^22p_{3/2}3d_{5/2}$	2	$1s^22s^22p^22p_{3/2}^2$	2	13.859	0.1			13.842	...	13.851	1
O19	$1s^22s^22p_{1/2}2p_{3/2}^2 3d_{5/2}$	3	$1s^22s^22p^22p_{3/2}^2$	2	13.807	0.4	13.795 (5)	0.5	13.798	13.796	13.795	3
	$1s^22s^22p_{1/2}2p_{3/2}^2 3d_{5/2}$	2	$1s^22s^22p_{1/2}2p_{3/2}^3$	2	13.815	<0.1			...	...	...	...
O20	$1s^22s^22p_{1/2}2p_{3/2}^2 3d_{3/2}$	1	$1s^22s^22p_{1/2}2p_{3/2}^3$	2	13.792	0.1	13.759 (5)	0.2	13.792	...	...	...
	$1s^22s^22p^22p_{3/2}3d_{3/2}$	1	$1s^22s^22p^22p_{3/2}^2$	0	13.780	<0.1			13.780	...	...	...
O21	$1s^22s^22p^22p_{3/2}^2 3d_{5/2}$	1	$1s^22s^22p^22p_{3/2}^2$	0	13.689	<0.1	13.676 (4)	0.2	...	...	...	...
	$1s^22s^22p_{1/2}2p_{3/2}^2 3d_{5/2}$	2	$1s^22s^22p_{1/2}2p^3$	2	13.687	<0.1			...	...	...	...
	$1s^22s^22p_{1/2}2p_{3/2}^2 3d_{3/2}$	2	$1s^22s^22p^22p_{3/2}^2$	2	13.682	0.1			13.672	...	...	...
	$1s^22s^22p_{1/2}2p_{3/2}^2 3d_{3/2}$	2	$1s^22s^22p_{1/2}2p_{3/2}^3$	1	13.675	0.1			13.670	13.670	13.669	3
	$1s^22s^22p_{1/2}2p_{3/2}^2 3d_{5/2}$	1	$1s^22s^22p_{1/2}2p_{3/2}^3$	1	13.674	<0.1			13.670	...	...	...
O22	$1s^22s^22p_{1/2}2p_{3/2}^2 3d_{3/2}$	3	$1s^22s^22p^22p_{3/2}^2$	2	13.658	0.2	13.645 (4)	0.2	13.650	...	13.648	
O23	$1s^22s^22p_{1/2}2p_{3/2}^2 3d_{5/2}$	2	$1s^22s^22p^22p_{3/2}^2$	2	13.570	0.1	13.551 (5)	0.2	...	...	...	...
O24	$1s^22s^22p^22p_{3/2}3d_{5/2}$	3	$1s^22s^22p^22p_{3/2}^2$	2	13.524	1.0	13.518 (2)	1	13.521	13.520	13.520	3
O25	$1s^22s^22p_{1/2}2p_{3/2}^2 3d_{3/2}$	2	$1s^22s^22p^22p_{3/2}^2$	2	13.515	0.5	13.497 (5)	0.3	13.507	13.500	13.504	3
O26	$1s^22s^22p_{1/2}2p_{3/2}^2 3d_{3/2}$	1	$1s^22s^22p^22p_{3/2}^2$	0	13.474	0.3	13.462 (3)	0.4	13.465	...	...	...
	$1s^22s^22p_{1/2}2p_{3/2}^2 3d_{3/2}$	1	$1s^22s^22p^22p_{3/2}^2$	2	13.474	0.2			13.465	13.460	13.464	3
O27	$1s^22s^22p_{1/2}2p_{3/2}^2 3d_{5/2}$	3	$1s^22s^22p^22p_{3/2}^2$	2	13.429	0.1	13.423 (4)	0.2	13.423	13.430	13.424	3
O28	$1s^22s_{1/2}2p^22p_{3/2}^2 3p_{3/2}$	3	$1s^22s^22p^22p_{3/2}^2$	2	13.030	0.1	13.022 (6)	0.1	13.020	...	...	...
O29	$1s^22s_{1/2}2p_{1/2}2p_{3/2}^3 3p_{3/2}$	3	$1s^22s^22p^22p_{3/2}^2$	2	12.940	0.1	12.933 (6)	0.1	12.931	12.945	12.990	3
O30	$1s^22s_{1/2}2p^22p_{3/2}^2 4s$	2	$1s^22s_{1/2}2p^22p_{3/2}^3$	2	11.311	<0.1	11.298 (10)	<0.1	11.311	11.311	...	...
O31	See Table 4	...	...	...	...	...	See Table 4	...	10.933	10.943	...	...
O32	$1s^22s^22p_{1/2}2p_{3/2}^2 4d_{5/2}$	3	$1s^22s^22p^22p_{3/2}^2$	2	10.826	0.1	10.816 (4)	0.2	...	10.826	10.824	3
	$1s^22s^22p_{1/2}2p_{3/2}^2 4d_{3/2}$	1	$1s^22s^22p_{1/2}2p_{3/2}^3$	2	10.826	<0.1			10.827	...	...	
	$1s^22s^22p_{1/2}2p_{3/2}^2 4d_{5/2}$	2	$1s^22s^22p_{1/2}2p_{3/2}^3$	2	10.822	<0.1			10.827	...	...	
	$1s^22s^22p_{1/2}2p_{3/2}^2 4d_{5/2}$	3	$1s^22s^22p_{1/2}2p_{3/2}^3$	2	10.815	<0.1			10.816	...	10.813	3
O33	$1s^22s^22p_{1/2}2p_{3/2}^2 4d_{5/2}$	2	$1s^22s^22p_{1/2}2p_{3/2}^3$	1	10.779	<0.1	10.765 (8)	<0.1	10.799	...	10.77	3
O34	$1s^22s^22p_{1/2}2p_{3/2}^2 4d_{3/2}$	3	$1s^22s^22p^22p_{3/2}^2$	2	10.694	<0.1	10.684 (8)	<0.1	10.684	10.694	10.684	3

[a] Phillips et al. 1999.

[b] Mewe et al. 1985.

[c] See § 3 for explanation of relative intensity.

REFERENCES.—References from Kelly 1987 compilation: (1) Boiko et al. 1978; (2) Kastner et al. 1977; (3) Bromage et al. 1977.

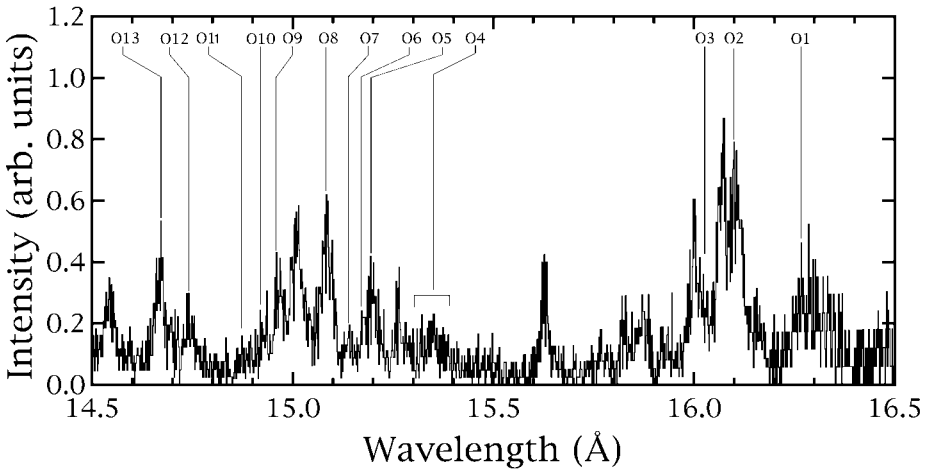

FIG. 2*a*

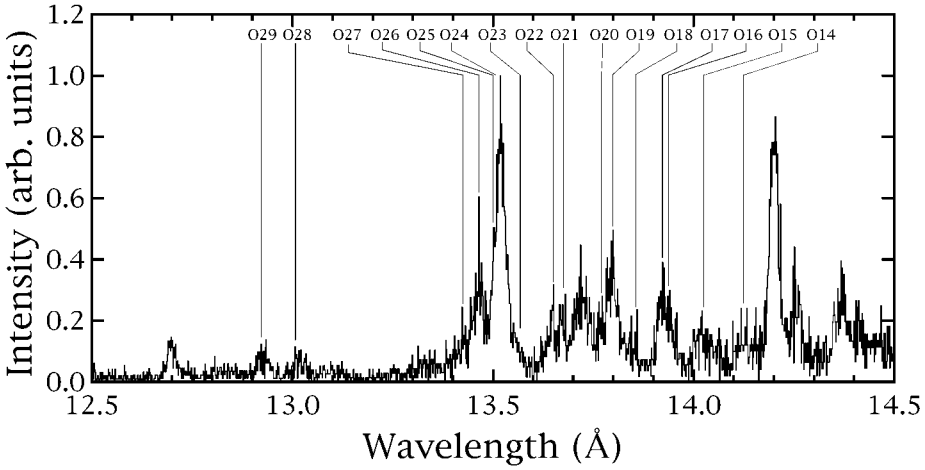

FIG. 2*b*

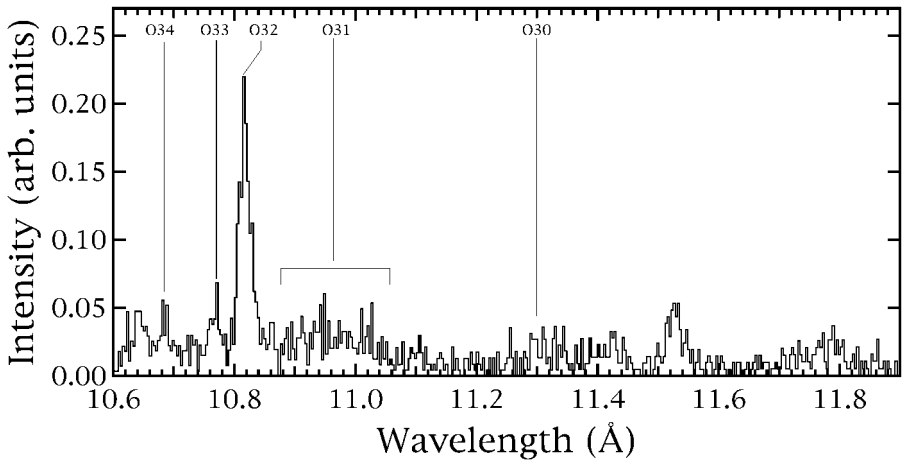

FIG. 2*c*

FIG. 2.—(*a*) Fe XIX spectrum between 14.5 and 16.5 Å normalized to O24. (*b*) Fe XIX spectrum between 12.5 and 14.5 Å normalized to O24. (*c*) Fe XIX spectrum between 10.6 and 11.9 Å normalized to O24. The scale is ~20% of the scale in (*a*) and (*b*).

3. WAVELENGTH DETERMINATION AND LINE IDENTIFICATION

Wavelengths were determined by taking advantage of the wavelength selective properties of crystals, i.e., Bragg's law, by which incident X-rays are dispersed into their constituent wavelengths. Once dispersed, their position is recorded by the PSPC and their wavelengths are determined relative to well known lines of helium- and hydrogen-like fluorine, oxygen, or neon as described by Beiersdorfer & Wargelin (1994) and Brown et al. (1998).

TABLE 4
LINES CONTRIBUTING TO O31 SPANNING 10.86–11.10 Å

HULLAC λ (Å)	Upper Configuration	J'	Lower Configuration	J	Intensity[a] (%)
11.1039	$1s^2 2s^2 2p^2 2p_{3/2} 4s$	1	$1s^2 2s^2 2p^2 2p_{3/2}^2$	2	2
11.0651	$1s^2 2s_{1/2} 2p_{1/2} 2p_{3/2}^3 4d_{3/2}$	1	$1s^2 2s_{1/2} 2p_{1/2} 2p^4$	1	1
11.0372	$1s^2 2s_{1/2} 2p^2 2p_{3/2}^2 4d_{5/2}$	1	$1s^2 2s_{1/2} 2p^2 2p_{3/2}^3$	2	1
11.0359	$1s^2 2s_{1/2} 2p^2 2p_{3/2}^2 4d_{5/2}$	3	$1s^2 2s_{1/2} 2p^2 2p_{3/2}^3$	2	7
11.0312	$1s^2 2s^2 2p^2 2p_{3/2} 4d_{5/2}$	2	$1s^2 2s_{1/2} 2p^2 2p_{3/2}^3$	2	4
10.9996	$1s^2 2s_{1/2} 2p_{1/2} 2p_{3/2}^3 4s$	2	$1s^2 2s_{1/2} 2p_{1/2} 2p^4$	1	2
10.9964	$1s^2 2s_{1/2} 2p_{1/2} 2p_{3/2}^3 4d_{5/2}$	2	$1s^2 2s_{1/2} 2p_{1/2} 2p^4$	1	2
10.9859	$1s^2 2s_{1/2} 2p_{1/2} 2p_{3/2}^3 4d_{3/2}$	3	$1s^2 2s_{1/2} 2p^2 2p_{3/2}^3$	2	2
10.9858	$1s^2 2s_{1/2} 2p_{1/2} 2p_{3/2}^3 4d_{3/2}$	2	$1s^2 2s_{1/2} 2p^2 2p_{3/2}^3$	2	1
10.9484	$1s^2 2s^2 2p_{1/2} 2p_{3/2}^2 4s_{1/2}$	2	$1s^2 2s^2 2p^2 2p_{3/2}^2$	2	1
10.9414	$1s^2 2s^2 2p^2 2p_{3/2} 4d_{5/2}$	2	$1s^2 2s^2 2p_{1/2} 2p_{3/2}^3$	1	12
10.9323	$1s^2 2s^2 2p^2 2p_{3/2} 4d_{5/2}$	1	$1s^2 2s^2 2p_{1/2} 2p_{3/2}^3$	1	3
10.9165	$1s^2 2s^2 2p^2 2p_{3/2} 4d_{5/2}$	1	$1s^2 2s^2 2p^2 2p_{3/2}^2$	0	9
10.9024	$1s^2 2s^2 2p_{1/2} 2p_{3/2}^2 4s$	3	$1s^2 2s^2 2p^2 2p_{3/2}^2$	2	3
10.8975	$1s^2 2s^2 2p^2 2p_{3/2} 4d_{5/2}$	3	$1s^2 2s^2 2p_{1/2} 2p_{3/2}^3$	2	2
10.8935	$1s^2 2s^2 2p_{1/2} 2p_{3/2}^2 4d_{3/2}$	3	$1s^2 2s^2 2p_{1/2} 2p_{3/2}^3$	2	2
10.8780	$1s^2 2s^2 2p_{1/2} 2p_{3/2}^2 4d_{5/2}$	2	$1s^2 2s^2 2p_{1/2} 2p_{3/2}^3$	2	1
10.8390	$1s^2 2s^2 2p^2 2p_{3/2} 4d_{5/2}$	2	$1s^2 2s^2 2p^2 2p_{3/2}^2$	2	10
10.8375	$1s^2 2s^2 2p_{1/2} 2p_{3/2}^2 4d_{5/2}$	1	$1s^2 2s^2 2p_{1/2} 2p_{3/2}^3$	2	1

NOTE.—The flux in this feature is equal to the flux in O32.
[a] Intensity predicted by HULLAC relative to line O32.

The results of our measurements are given in Tables 2–10, and the corresponding spectra are shown in Figures 1–7. Each table gives the line label used in the figures in the first column, which is the elemental symbol for the charge state followed by a number. For example, F1 is from fluorine-like Fe XVIII. The number is for denotation purposes only. The spectra in Figures 1–7 are the concatenation of the spectra measured at each crystal position. The wavelengths where the spectra are joined together are given in Table 1. The second through seventh columns give the data provided by the Hebrew University-Lawrence Livermore Atomic Code (HULLAC), which consists of the following: the upper level's configuration including the total angular momentum of the open subshells, the total angular momentum (J'), and the lower level's configuration including the total angular momentum of the open subshells, and total angular momentum (J), the transition wavelength, and the relative intensity. HULLAC employs the multiconfigurational relativistic parametric-potential method to calculate wave functions, transition probabilities, and energies (Klapisch et al. 1977). In addition, HULLAC uses the factorization-interpolation method to calculate relativistic distorted-wave collisional excitation cross sections (Bar-Shalom, Klapisch, & Oreg 1988). HULLAC, thus, employs a consistent set of wavefunctions to generate the atomic parameters necessary to build a model spectrum.

The eighth column in our tables gives our measured wavelength in Å of the feature most likely to correspond to the given HULLAC transition. These identifications are based on wavelengths, comparison of relative intensities, and the ability of EBIT-II to isolate a single charge state. The uncertainty in each measured wavelength is given in parenthesis in mÅ next to each value. The uncertainty is based on counting statistics in both the measured lines and the calibration lines as well as a derived uncertainty in the overall calibration.

The ninth column gives the measured intensity (photon count rate) of each line relative to the strongest line in the charge state. These values are reliable to within a factor of 2 across the entire spectrum and to within ≈20% for lines that are less than 0.3 Å apart, unless there is a concatenation wavelength between them (see Table 1). The efficiency of the spectrometer, including the response of all foils and crystals, has been accounted for in these measurements. The large uncertainty across the spectra is a result of the fact that the lines used for normalization from one spectrum to the next were sometimes weak or from a charge state other than the one being measured.

The tenth column gives the wavelengths of Phillips et al. (1999) chosen based on the analysis of *SMM* data; the eleventh column gives the values found in MEKA (Mewe, Gronenschild, & van den Oord 1985). The twelfth column is composed of the wavelengths compiled in the Kelly tables (Kelly 1987). References to the specific work from which each Kelly wavelength was taken is given in the thirteenth column. Most of these references consist of results from laser produced plasmas which have substantially higher densities than most astrophysical sources, tokamak plasmas, or electron beam ion traps.

Several emission features consist of lines that are less than 10 mÅ apart. These blends are generally indistinguishable from single line features. Tables 2–10 include all predicted lines which may contribute to each measured feature. Also measured are features consisting of many densely spaced lines forming wide features, which may span several tens of mÅ. In some cases the number of predicted lines that contribute to these features are given in a separate table. The measured flux in these blended features is also given relative

TABLE 5

COMPARISON OF MEASUREMENTS AND CALCULATIONS OF Fe XX LINES

	HULLAC						THIS MEASUREMENT		PHILLIPS[a]	MEKA[b]	KELLY 1987	
LABEL	Upper	J'	Lower	J	λ (Å)	I	λ (Å)	I[c]	λ (Å)	λ (Å)	λ (Å)	Reference
N1.....	$1s^22s^22p_{1/2}2p_{3/2}3p_{3/2}$	$\frac{7}{2}$	$1s^22s_{1/2}2p_{1/2}2p_{3/2}^3$	$\frac{5}{2}$	15.560	<0.1	15.517 (10)	0.1	...	...	...	...
N2.....	$1s^22s^22p_{1/2}2p_{3/2}3p_{1/2}$	$\frac{1}{2}$	$1s^22s_{1/2}2p_{1/2}^2p_{3/2}^2$	$\frac{3}{2}$	15.164	<0.1	15.146 (9)	0.1		...	...	...
	$1s^22s^22p_{3/2}^23p_{1/2}$	$\frac{5}{2}$	$1s^22s_{1/2}2p_{1/2}2p_{3/2}^3$	$\frac{5}{2}$	15.159	<0.1			...	...	...	...
N3.....	$1s^22s^22p_{1/2}^23p_{3/2}$	$\frac{3}{2}$	$1s^22s_{1/2}2p_{1/2}^2p_{3/2}^2$	$\frac{5}{2}$	15.055	0.1	15.047 (7)	0.2	15.146[d]	...	...	...
	$1s^22s^22p_{1/2}2p_{3/2}3p_{3/2}$	$\frac{5}{2}$	$1s^22s_{1/2}2p_{1/2}^2p_{3/2}^2$	$\frac{3}{2}$	15.073	<0.1		0.2	...	...	...	...
N4.....	$1s^22s^22p_{1/2}2p_{3/2}3p_{3/2}$	$\frac{3}{2}$	$1s^22s_{1/2}2p_{1/2}2p_{3/2}^3$	$\frac{1}{2}$	14.970	0.1	14.99–14.89	0.1	15.002[e]			...
	$1s^22s^22p_{1/2}2p_{3/2}3p_{1/2}$	$\frac{3}{2}$	$1s^22s_{1/2}2p^22p_{3/2}^2$	$\frac{5}{2}$	14.946	0.1			15.002			...
	$1s^22s^22p_{1/2}2p_{3/2}3p_{3/2}$	$\frac{3}{2}$	$1s^22s_{1/2}2p^22p_{3/2}^2$	$\frac{3}{2}$	14.919	0.1						...
	$1s^22s^22p_{1/2}2p_{3/2}3p_{1/2}$	$\frac{3}{2}$	$1s^22s_{1/2}2p_{1/2}2p_{3/2}^3$	$\frac{1}{2}$	14.915	0.1			...	...	...	...
	$1s^22s^22p_{1/2}2p_{3/2}3p_{1/2}$	$\frac{5}{2}$	$1s^22s_{1/2}2p^22p_{3/2}^2$	$\frac{5}{2}$	14.878	<0.1	14.89–14.80	0.1				...
N5.....	$1s^22s^22p_{1/2}2p_{3/2}3p_{3/2}$	$\frac{3}{2}$	$1s^22s_{1/2}2p^22p_{3/2}^2$	$\frac{3}{2}$	14.864	<0.1			...	...	...	...
	$1s^22s^22p_{1/2}2p_{3/2}3p_{3/2}$	$\frac{3}{2}$	$1s^22s_{1/2}2p^22p_{3/2}^2$	$\frac{5}{2}$	14.852	<0.1			...	...	...	...
	$1s^22s^22p_{1/2}2p_{3/2}3p_{3/2}$	$\frac{7}{2}$	$1s^22s_{1/2}2p^22p_{3/2}^2$	$\frac{5}{2}$	14.827	<0.1			...	...	...	...
N6.....	$1s^22s^22p_{1/2}2p_{3/2}3p_{3/2}$	$\frac{3}{2}$	$1s^22s_{1/2}2p_{1/2}^2p_{3/2}^2$	$\frac{5}{2}$	14.776	0.2	14.754 (7)	0.1	14.799[f]	...	...	...
N7.....	$1s^22s_{1/2}2p^22p_{3/2}3s_{1/2}$	$\frac{3}{2}$	$1s^22s_{1/2}2p_{1/2}2p_{3/2}^3$	$\frac{1}{2}$	14.466	0.1	14.460 (8)	0.1	14.457	...	...	...
	$1s^22s^22p_{3/2}^23p_{3/2}$	$\frac{3}{2}$	$1s^22s_{1/2}2p_{1/2}^2p_{3/2}^2$	$\frac{3}{2}$	14.465	0.1	14.460 (8)	0.1	14.457	...	...	...
N8.....	$1s^22s_{1/2}2p^22p_{3/2}3s_{1/2}$	$\frac{3}{2}$	$1s^22s_{1/2}2p^22p_{3/2}^2$	$\frac{3}{2}$	14.419	<0.1	14.42–14.3	0.2	14.407	...	...	...
	$1s^22s_{1/2}2p^22p_{3/2}3s_{1/2}$	$\frac{3}{2}$	$1s^22s_{1/2}2p_{1/2}2p_{3/2}^3$	$\frac{3}{2}$	14.367	<0.1			...	...	...	...
	$1s^22s^22p_{3/2}^23p_{3/2}$	$\frac{3}{2}$	$1s^22s_{1/2}2p^22p_{3/2}^2$	$\frac{5}{2}$	14.330	<0.1			...	...	...	...
N9.....	$1s^22s_{1/2}2p^22p3s_{1/2}$	$\frac{3}{2}$	$1s^22s_{1/2}2p_{1/2}^2p_{3/2}^2$	$\frac{5}{2}$	14.285	0.3	14.267 (4)	0.2	14.260	...	...	...
N10.....	$1s^22s_{1/2}2p_{1/2}2p_{3/2}^23s_{1/2}$	$\frac{3}{2}$	$1s^22s_{1/2}2p_{1/2}^2p_{3/2}^2$	$\frac{1}{2}$	14.158	<0.1	14.163 (5)	<0.1	...	...	...	...
N11.....	$1s^22s^22p_{1/2}2p_{3/2}3s_{1/2}$	$\frac{1}{2}$	$1s^22s^22p_{1/2}2p_{3/2}^2$	$\frac{3}{2}$	14.072	<0.1	14.062 (6)	<0.1	...	...	14.014	1
	$1s^22s^22p_{1/2}2p_{3/2}3s_{1/2}$	$\frac{3}{2}$	$1s^22s^22p_{1/2}2p_{3/2}^2$	$\frac{5}{2}$	14.062	<0.1	14.062 (6)	<0.1	14.071	...	14.009	1
N12.....	$1s^22s^22p_{1/2}^23s_{1/2}$	$\frac{1}{2}$	$1s^22s^22p^22p_{3/2}$	$\frac{3}{2}$	13.986	0.1	13.962 (6)	0.1	...	...	13.945	1
N13.....	$1s^22s^22p_{1/2}2p_{3/2}3s_{1/2}$	$\frac{3}{2}$	$1s^22s^22p^22p_{3/2}$	$\frac{3}{2}$	13.860	0.2	13.843 (6)	0.1	...	...	13.818	1
N14.....	$1s^22s^22p_{1/2}2p_{3/2}3s_{1/2}$	$\frac{5}{2}$	$1s^22s^22p^22p_{3/2}$	$\frac{3}{2}$	13.774	0.1	13.767 (5)	0.2	13.731	...	13.770	1
N15.....	$1s^22s_{1/2}2p^22p_{3/2}3d_{5/2}$	$\frac{5}{2}$	$1s^22s_{1/2}2p_{1/2}^2p_{3/2}^2$	$\frac{3}{2}$	13.527	0.1			...	...	13.464	1
	$1s^22s_{1/2}2p^22p_{3/2}3d_{5/2}$	$\frac{3}{2}$	$1s^22s_{1/2}2p_{1/2}^2p_{3/2}^2$	$\frac{3}{2}$	13.523	<0.1	13.535 (3)	0.4	...	...	...	...
N16.....	$1s^22s_{1/2}2p_{1/2}2p_{3/2}^23s_{1/2}$	$\frac{3}{2}$	$1s^22s_{1/2}2p_{1/2}2p_{3/2}^3$	$\frac{1}{2}$	13.459	<0.1	13.444 (5)	0.1	...	...	...	...
N17.....	$1s^22s^22p_{1/2}2p_{3/2}3d_{3/2}$	$\frac{3}{2}$	$1s^22s^22p_{1/2}2p_{3/2}^2$	$\frac{1}{2}$	13.432	<0.1	13.40–13.38	0.1	...	...	...	...
	$1s^22s_{1/2}2p_{1/2}2p_{3/2}^23s_{1/2}$	$\frac{3}{2}$	$1s^22s_{1/2}2p^22p_{3/2}^2$	$\frac{3}{2}$	13.418	0.1			...	...	...	...
	$1s^22s_{1/2}2p^22p_{3/2}3d_{5/2}$	$\frac{5}{2}$	$1s^22s_{1/2}2p^22p_{3/2}^2$	$\frac{5}{2}$	13.408	<0.1			...	...	...	...
N18.....	$1s^22s_{1/2}2p_{1/2}2p_{3/2}^23d_{5/2}$	$\frac{7}{2}$	$1s^22s_{1/2}2p_{1/2}^2p_{3/2}^2$	$\frac{5}{2}$	13.396	0.2	13.385 (4)	0.2	13.407	...	13.361	1
N19.....	$1s^22s^22p^23d_{3/2}$	$\frac{3}{2}$	$1s^22s^22p_{1/2}2p_{3/2}^2$	$\frac{3}{2}$	13.349	<0.1	13.347 (9)	0.1	...	...	...	...
N20.....	$1s^22s^22p^23d_{5/2}$	$\frac{5}{2}$	$1s^22s^22p_{1/2}2p_{3/2}^2$	$\frac{3}{2}$	13.308	<0.1	13.34–13.28	<0.1	13.308	...	...	...
	$1s^22s_{1/2}2p_{1/2}2p_{3/2}^23s_{1/2}$	$\frac{3}{2}$	$1s^22s_{1/2}2p^22p_{3/2}^2$	$\frac{5}{2}$	13.302	<0.1			...	...	...	...
	$1s^22s^22p_{1/2}2p_{3/2}3d_{3/2}$	$\frac{3}{2}$	$1s^22s^22p_{1/2}2p_{3/2}^2$	$\frac{5}{2}$	13.293	<0.1						...
	$1s^22s^22p_{1/2}2p_{3/2}3d_{5/2}$	$\frac{7}{2}$	$1s^22s^22p_{1/2}2p_{3/2}^2$	$\frac{5}{2}$	13.290	0.1			...	...	...	...
N21.....	$1s^22s^22p_{1/2}2p_{3/2}3d_{5/2}$	$\frac{1}{2}$	$1s^22s^22p_{1/2}2p_{3/2}^2$	$\frac{1}{2}$	13.275	0.1	13.274 (6)	0.1	13.265	...	...	...
	$1s^22s^22p_{1/2}2p_{3/2}3d_{3/2}$	$\frac{1}{2}$	$1s^22s^22p_{1/2}2p_{3/2}^2$	$\frac{1}{2}$	13.262	<0.1			...	...	...	...
N22.....	$1s^22s^22p_{1/2}2p_{3/2}3d_{3/2}$	$\frac{7}{2}$	$1s^22s^22p_{1/2}2p_{3/2}^2$	$\frac{5}{2}$	13.223	<0.1	13.213 (10)	0.1	...	...	...	...
	$1s^22s^22p_{1/2}2p_{3/2}3d_{3/2}$	$\frac{5}{2}$	$1s^22s^22p_{1/2}2p_{3/2}^2$	$\frac{5}{2}$	13.223	<0.1			...	...	...	...
	$1s^22s^22p_{1/2}2p_{3/2}3d_{3/2}$	$\frac{3}{2}$	$1s^22s^22p_{1/2}2p_{3/2}^2$	$\frac{3}{2}$	13.221	<0.1			...	...	...	...
	$1s^22s^22p_{1/2}2p_{3/2}3d_{3/2}$	$\frac{5}{2}$	$1s^22s^22p_{1/2}2p_{3/2}^2$	$\frac{3}{2}$	13.203	<0.1			...	...	...	...
	$1s^22s^22p_{1/2}2p_{3/2}3d_{5/2}$	$\frac{3}{2}$	$1s^22s^22p_{1/2}2p_{3/2}^2$	$\frac{1}{2}$	13.195	<0.1			...	...	...	...
	$1s^22s_{1/2}2p^22p_{3/2}3p_{1/2}$	$\frac{3}{2}$	$1s^22s^22p_{1/2}2p_{3/2}^2$	$\frac{1}{2}$	13.188	<0.1			...	...	...	...
N23.....	$1s^22s^22p_{1/2}2p_{3/2}3d_{5/2}$	$\frac{5}{2}$	$1s^22s^22p_{1/2}2p_{3/2}^2$	$\frac{5}{2}$	13.162	0.1	13.153 (7)	0.1	13.160	...	13.138	1
	$1s^22s^22p_{1/2}2p_{3/2}3d_{5/2}$	$\frac{3}{2}$	$1s^22s^22p_{1/2}2p_{3/2}^2$	$\frac{3}{2}$	13.161	0.1			13.160	...	...	...
N24.....	$1s^22s^22p_{1/2}2p_{3/2}3d_{5/2}$	$\frac{5}{2}$	$1s^22s^22p_{1/2}2p_{3/2}^2$	$\frac{3}{2}$	13.153	0.2	13.137 (13)	<0.1	13.144[g]	...	...	...

TABLE 5—*Continued*

	HULLAC						This Measurement		Phillips[a]	MEKA[b]	Kelly 1987	
Label	Upper	J'	Lower	J	λ (Å)	I	λ (Å)	I[c]	λ (Å)	λ (Å)	λ (Å)	Reference
	$1s^22s^22p_{1/2}2p_{3/2}3d_{3/2}$	$\frac{3}{2}$	$1s^22s^22p_{1/2}2p^2_{3/2}$	$\frac{5}{2}$	13.142	<0.1		<0.1	...	...	...	...
N25.....	$1s^22s^22p^2_{1/2}3d_{3/2}$	$\frac{3}{2}$	$1s^22s^22p^2_{3/2}$	$\frac{3}{2}$	13.101	<0.1	13.100 (7)	0.1	...	...	...	...
	$1s^22s^22p_{1/2}2p_{3/2}3d_{5/2}$	$\frac{7}{2}$	$1s^22s^22p_{1/2}2p^2_{3/2}$	$\frac{5}{2}$	13.100	<0.1			...	...	...	...
N26.....	$1s^22s^22p^2_{1/2}3d_{5/2}$	$\frac{5}{2}$	$1s^22s^22p^2_{3/2}$	$\frac{3}{2}$	13.062	0.2	13.061 (6)	0.1	13.053	...	...	...
N27.....	$1s^22s_{1/2}2p^22p_{3/2}3p_{3/2}$	$\frac{7}{2}$	$1s^22s^22p_{1/2}2p^2_{3/2}$	$\frac{5}{2}$	13.011	0.1	13.024 (8)	0.1	...	...	...	...
	$1s^22s_{1/2}2p_{1/2}2p^2_{3/2}3d_{5/2}$	$\frac{7}{2}$	$1s^22s_{1/2}2p_{1/2}2p^3_{3/2}$	$\frac{5}{2}$	13.015	0.1			12.995	...	...	...
N28.....	$1s^22s^22p_{1/2}2p_{3/2}3d_{3/2}$	$\frac{5}{2}$	$1s^22s^22p_{1/2}2p^2_{3/2}$	$\frac{3}{2}$	12.988	0.1	12.992 (6)	0.1	12.995	...	12.983	2
	$1s^22s^22p_{1/2}2p_{3/2}3d_{3/2}$	$\frac{3}{2}$	$1s^22s^22p^22p_{3/2}$	$\frac{3}{2}$	12.978	0.1			12.983	...	...	...
N29.....	$1s^22s^22p_{1/2}2p_{3/2}3d_{3/2}$	$\frac{5}{2}$	$1s^22s^22p^22p_{3/2}$	$\frac{3}{2}$	12.960	0.3	12.965 (5)	0.2	12.965	12.953	...	...
N30.....	$1s^22s^22p_{1/2}2p_{3/2}3d_{5/2}$	$\frac{5}{2}$	$1s^22s^22p^22p_{3/2}$	$\frac{3}{2}$	12.912	0.3	12.90–12.93	0.1	12.904	12.912	12.946	1
	$1s^22s^22p^2_{3/2}3d_{3/2}$	$\frac{7}{2}$	$1s^22s^22p_{1/2}2p^2_{3/2}$	$\frac{5}{2}$	12.894	0.1	...		...	...	12.888	1
N31[h]	$1s^22s^22p_{1/2}2p_{3/2}3d_{5/2}$	$\frac{5}{2}$	$1s^22s^22p^22p_{3/2}$	$\frac{3}{2}$	12.854	0.8	12.864 (4)	1	12.847	12.847	...	...
	$1s^22s^22p_{1/2}2p_{3/2}3d_{3/2}$	$\frac{3}{2}$	$1s^22s^22p^22p_{3/2}$	$\frac{3}{2}$	12.834	1.0	12.846 (3)	1	12.827	12.827	12.818	1
	$1s^22s^22p_{1/2}2p_{3/2}3d_{3/2}$	$\frac{1}{2}$	$1s^22s^22p^22p_{3/2}$	$\frac{3}{2}$	12.819	0.4	12.824 (4)	1	12.813	12.812	...	...
N32.....	$1s^22s_{1/2}2p_{1/2}2p^2_{3/2}3d_{5/2}$	$\frac{5}{2}$	$1s^22s_{1/2}2p^2_{1/2}2p^2_{3/2}$	$\frac{3}{2}$	12.610	<0.1	12.621 (8)	<0.1	...	...	...	...
N33.....	$1s^22s_{1/2}2p_{1/2}2p^2_{3/2}3p_{1/2}$	$\frac{3}{2}$	$1s^22s^22p^22p_{3/2}$	$\frac{3}{2}$	12.602	0.1	12.576 (5)	0.1	12.600	...	...	...
	$1s^22s_{1/2}2p^3_{3/2}3p_{1/2}$	$\frac{5}{2}$	$1s^22s^22p^22p_{3/2}$	$\frac{3}{2}$	12.602	0.2	12.576 (5)		12.600	...	...	...
N34.....	$1s^22s_{1/2}2p^22p_{3/2}3p_{1/2}$	$\frac{1}{2}$	$1s^22s^22p^22p_{3/2}$	$\frac{3}{2}$	12.591	0.1	12.526 (8)	<0.1	12.580	...	...	...
N35.....	$1s^22s_{1/2}2p_{1/2}2p^2_{3/2}3d_{5/2}$	$\frac{7}{2}$	$1s^22s_{1/2}2p^2_{1/2}2p^2_{3/2}$	$\frac{5}{2}$	12.498	<0.1	12.468 (9)	<0.1	...	...	...	...
N36.....	$1s^22s_{1/2}2p_{1/2}2p^2_{3/2}3p_{1/2}$	$\frac{3}{2}$	$1s^22s^22p^22p_{3/2}$	$\frac{3}{2}$	11.786	<0.1	11.796 (10)	<0.1	11.787	...	...	...
N37.....	$1s^22s_{1/2}2p^22p_{3/2}3p_{3/2}$	$\frac{5}{2}$	$1s^22s^22p^22p_{3/2}$	$\frac{3}{2}$	11.754	<0.1	11.762 (5)	<0.1	11.760	...	...	...
N38.....	$1s^22s_{1/2}2p_{1/2}2p^2_{3/2}3p_{3/2}$	$\frac{1}{2}$	$1s^22s^22p^22p_{3/2}$	$\frac{3}{2}$	11.730	<0.1	11.732 (7)	<0.1	...	...	...	...

[a] Phillips et al. 1999.
[b] Mewe et al. 1985.
[c] See § 3 for explanation of relative intensity.
[d] Phillips et al. identify this line with the transition given by N3, predicted by HULLAC at 15.055 Å, although it equals the measured wavelength of N2.
[e] Phillips et al. identify this line with a $J' = \frac{5}{2} \rightarrow J = \frac{1}{2}$ transition.
[f] Phillips et al. identify this line with a $J' = \frac{5}{2} \rightarrow J = \frac{5}{2}$ transition.
[g] Phillips et al. identify this line with a $J' = \frac{7}{2} \rightarrow J = \frac{3}{2}$ transition.
[h] The ratio of the lines 12.864, 12.846, and 12.824 Å is ~1 : 2 : 1. The intensity of all lines in this charge state are given relative to the summed intensity of these three lines, i.e., the entire N31 feature.

References.—References from Kelly 1987 compilation: (1) Bromage et al. 1977; (2) Boiko et al. 1978.

to the nearest strong line feature. Below is a description of the emission from each of the individual iron ions.

3.1. *Fluorine-Like* Fe XVIII

The Fe XVIII spectrum is shown in Figure 1 with the corresponding wavelengths and identifications in Table 2. We have identified 36 features belonging to this charge state between 11.0 and 17.7 Å. Most result from transitions originating in an $n = 3$ configuration, but we also identify nine features whose transitions originate in an $n = 4$ configuration.

3.1.1. 14 Å $\leq \lambda \leq$ 18 Å: *F1–F21*

The strongest L-shell line emission from Fe XVIII occurs in this wavelength band. These include transitions of the type $3s \rightarrow 2p$ and $3d \rightarrow 2p$. In particular, the lines at 16.16, 16.07, 16.00, 15.87, 15.82, and 15.63 Å, labeled F3, 4, 6, 8, 9, and F11, respectively, represent the stronger lines originating in a $3s$ configuration; and the lines at 14.53, 14.37, 14.26, and 14.21 Å, labeled F15, 17, 19, and F20, represent the stronger lines originating in a $3d$ configuration. The wavelengths of all of these lines are overestimated by HULLAC by ~10–40 mÅ. The values adopted by Phillips et al. (1999) and those reported in the Kelly tables are all within 6 mÅ.

The F1 line at 17.62 Å (see Fig. 1*a*) is of particular interest owing to a long history of uncertainty related to its identification in solar spectra. This line had been tentatively identified as Fe Lyα (McKenzie et al. 1980); however, the laboratory value of 17.59 ± 0.02 Å for this characteristic line (Bearden 1967) is in disagreement with the wavelength McKenzie et al. (1980) reported from the solar measurement. This fact, coupled with a calculation showing that the fluorescence of Fe Lyα does not produce enough flux to account for the observed feature in the solar spectra, made this identification doubtful (McKenzie & Landecker 1982). Acton et al. (1985) completely rejected the Fe Lyα "identification" on the basis of both incorrect wavelength and incorrect line shape. They suggested that this line is the

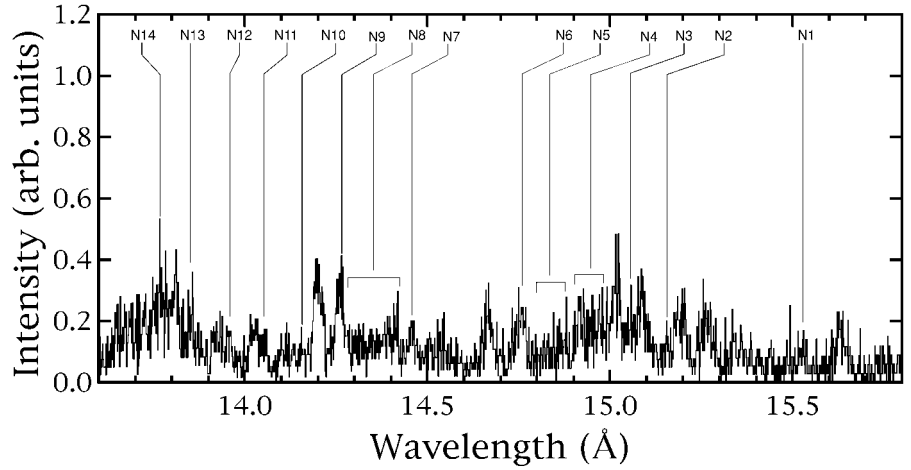

FIG. 3*a*

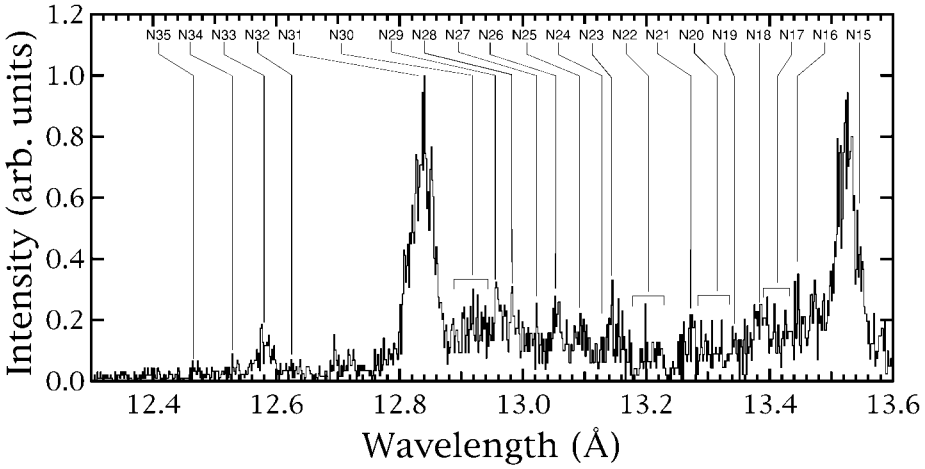

FIG. 3*b*

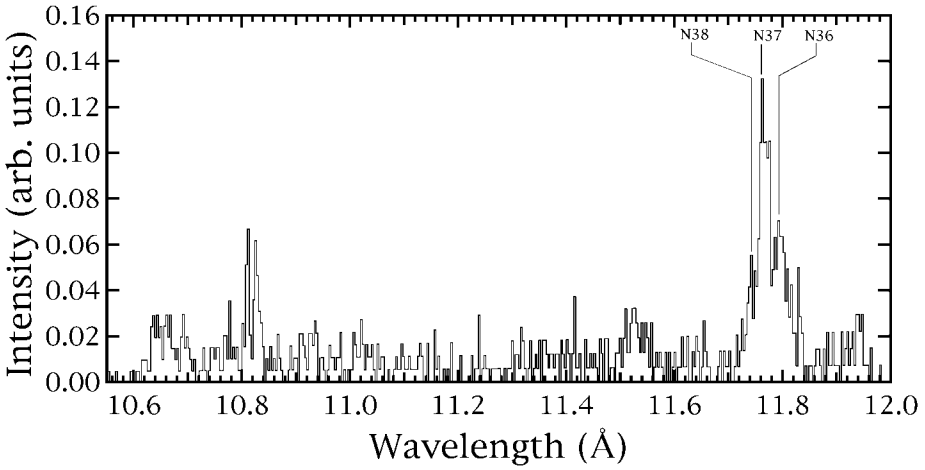

FIG. 3*c*

FIG. 3.—(*a*) Fe XX spectrum between 13.6 and 15.8 Å normalized to N31. (*b*) Fe XX spectrum between 12.3 and 13.6 Å normalized to N31. (*c*) Fe XX spectrum between 10.6 and 12.0 Å normalized to N31.

unclassified iron line seen in the low-inductance vacuum spark spectrum of Cohen & Feldman (1970). Our measurement, together with the calculations by HULLAC and Cornille et al. (1992) show that this line is the $1s^2 2s^2_{1/2} 2p_{1/2} 2p^3_{3/2} 3p_{1/2} \quad J = \frac{3}{2} \rightarrow 1s^2 2s_{1/2} 2p^2_{1/2} 2p^4_{3/2} \quad J = \frac{1}{2}$ Fe XVIII line. This line is a result of configuration mixing and, therefore, is only predicted by models which are multiconfigurational. A thorough explanation of this identifica-

TABLE 6

COMPARISON OF MEASUREMENTS AND CALCULATIONS OF Fe XXI LINES

	HULLAC						THIS MEASUREMENT		PHILLIPS[a]	MEKA[b]	KELLY 1987	
LABEL	Upper	J′	Lower	J	λ (Å)	I	λ (Å)	I[c]	λ (Å)	λ (Å)	λ (Å)	Reference
C1	$1s^2 2s^2 2p_{1/2} 3p_{1/2}$	0	$1s^2 2s_{1/2} 2p^2 2p_{3/2}$	1	14.029	0.2	14.008(15)	0.3	13.993	...	...	...
C2	$1s^2 2s^2 2p_{3/2} 3p_{3/2}$	0	$1s^2 2s_{1/2} 2p^2 2p_{3/2}$	1	13.618	<0.1	13.574(6)	0.1	...	...	...	...
C3	$1s^2 2s_{1/2} 2p^2 3s_{1/2}$	0	$1s^2 2s_{1/2} 2p^2 2p_{3/2}$	1	13.521	0.2	13.507(5)	0.5	13.530	...	...	...
C4	$1s^2 2s_{1/2} 2p_{1/2} 2p_{3/2} 3d_{5/2}$	2	$1s^2 2s_{1/2} 2p^2 2p_{3/2}$	1	12.835	0.1	12.822(5)	0.5	12.817	...	...	...
C5	$1s^2 2s_{1/2} 2p_{1/2} 2p_{3/2} 3d_{5/2}$	2	$1s^2 2s_{1/2} 2p_{1/2} 2p^2_{3/2}$	1	12.674	<0.1	12.649(8)	0.1	...	...	...	...
C6	$1s^2 2s^2 2p_{1/2} 3d_{5/2}$	3	$1s^2 2s^2 2p_{1/2} 2p_{3/2}$	2	12.510	0.1	12.499(4)	0.2	12.501	12.530	...	...
C7	$1s^2 2s^2 2p_{1/2} 3d_{5/2}$	2	$1s^2 2s^2 2p_{1/2} 2p_{3/2}$	1	12.429	0.1	12.422(5)	0.1	12.430	12.460	12.429[d]	1
C8	$1s^2 2s^2 2p_{1/2} 3d_{3/2}$	1	$1s^2 2s^2 2p_{1/2} 2p_{3/2}$	1	12.401	0.2	12.393(5)	0.2	12.399	12.400	...	...
C9	$1s^2 2s^2 2p_{3/2} 3d_{5/2}$	3	$1s^2 2s^2 2p_{1/2} 2p_{3/2}$	2	12.333	0.1	12.327(7)	0.1	...	12.380	...	...
	$1s^2 2s^2 2p_{3/2} 3d_{5/2}$	2	$1s^2 2s^2 2p_{1/2} 2p_{3/2}$	2	12.312	<0.1		0.1	12.312	...	...	...
C10	$1s^2 2s^2 2p_{1/2} 3d_{3/2}$	1	$1s^2 2s^2 2p^2$	0	12.292	1.0	12.284(2)	1	12.286	12.285	...	...
C11	$1s^2 2s_{1/2} 2p_{1/2} 2p_{3/2} 3d_{3/2}$	2	$1s^2 2s_{1/2} 2p^2_{1/2} 2p_{3/2}$	1	12.202	<0.1	12.204(8)	0.1	...	...	...	...
C12	$1s^2 2s_{1/2} 2p_{1/2} 2p_{3/2} 3p_{3/2}$	1	$1s^2 2s^2 2p_{1/2} 2p_{3/2}$	1	12.050	<0.1	12.044(9)	<0.1	...	...	12.201[e]	1
C13	$1s^2 2s_{1/2} 2p^2 3p_{3/2}$	1	$1s^2 2s^2 2p^2$	0	11.991	0.1	11.975(6)	0.1	11.974	...	...	...

[a] Phillips et al. 1999.
[b] Mewe et al. 1985.
[c] See § 3 for explanation of relative intensity.
[d] Bromage et al. have identified this as $J' = 1 \rightarrow J = 2$.
[e] Bromage et al. have identified this as $J' = 3 \rightarrow J = 3$.

REFERENCES.—References from Kelly 1987 compilation: (1) Bromage et al. 1977.

tion, including our measurement, is given by Drake et al. (1999).

The F20 line at 14.208 ± 0.003 Å is the strongest feature emitted from this charge state. Two predicted lines may be responsible for this feature: 14.203 and 14.216 Å. The 14.203 Å line is the stronger of the two predicted transitions; the 14.216 Å line is predicted to be approximately half as intense. The resolving power necessary to distinguish between these lines is ≈1000. Unfortunately, the two components are not resolved by our present measurement; nor are they resolved by the spectrometers on either *CXO* or *XMM* satellites whose resolving powers are $\lambda/\Delta\lambda \simeq 600$ and $\lambda/\Delta\lambda \simeq 450$, respectively, at this wavelength.

There are a few lines in this region that are not from transitions in the Fe XVIII ion. The stronger Fe XVII features are labeled in the notation of Parkinson (1973), i.e., 3C, 3D, 3E, 4C, 4D, 3G, and M2. The features that fall between 3C and F13 are the onset of stronger Fe XIX features such as O12 and O13 (see Table 3 and Fig. 2).

3.1.2. 11 Å ≤ λ ≤ 14 Å: *F22–F36*

This wavelength range contains transitions of the type $3p \rightarrow 2s$, $4d \rightarrow 2p$, and those involving two photon processes originating in a $3d$, $3p$, or $4d$ configuration such as F22, F25, and F30, respectively. As a result of the diminishing spectral resolution with decreasing Bragg angle and an increase in line density, several of the features identified in this region consist of blends.

It was not possible to assign a specific transition to F29 because there are too many similar type transitions in close proximity predicted by HULLAC. The four transitions predicted to be responsible for this feature are given in Table 2.

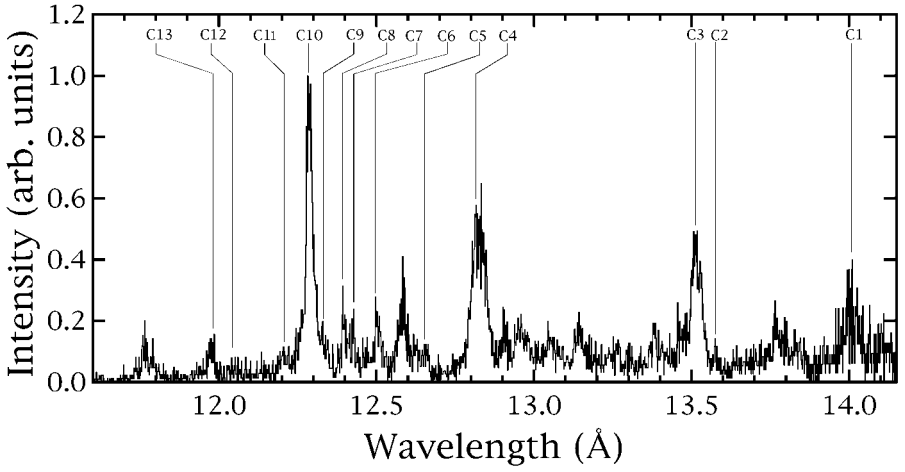

FIG. 4.—Fe XXI spectrum between 11.6 and 14.15 Å normalized to C10

TABLE 7

COMPARISON OF MEASUREMENTS AND CALCULATIONS OF Fe XXII LINES

	HULLAC						THIS MEASUREMENT		PHILLIPS[a]	MEKA[b]	KELLY 1987	
LABEL	Upper	J'	Lower	J	λ (Å)	I	λ (Å)	I[c]	λ (Å)	λ (Å)	λ (Å)	Reference
B1	$1s^22s^23p_{1/2}$	$\frac{1}{2}$	$1s^22s_{1/2}2p_{1/2}2p_{3/2}$	$\frac{3}{2}$	13.251	0.2	13.236(3)	0.2	13.243	...	...	...
B2	$1s^22s^23p_{3/2}$	$\frac{3}{2}$	$1s^22s_{1/2}2p_{3/2}^2$	$\frac{5}{2}$	13.232	<0.1	13.217(5)	0.1	...	...	...	...
B3	$1s^22s_{1/2}2p_{1/2}3s_{1/2}$	$\frac{1}{2}$	$1s^22s_{1/2}2p_{1/2}2p_{3/2}$	$\frac{1}{2}$	12.973	0.1	12.953(4)	0.2	12.986	...	...	...
B4	$1s^22s_{1/2}2p_{1/2}3s_{1/2}$	$\frac{1}{2}$	$1s^22s_{1/2}2p_{1/2}2p_{3/2}$	$\frac{3}{2}$	12.773	0.4	12.754(4)	0.3	12.763	...	...	...
B5	$1s^22s_{1/2}2p_{1/2}3d_{5/2}$	$\frac{5}{2}$	$1s^22s_{1/2}2p_{1/2}2p_{3/2}$	$\frac{3}{2}$	12.221	0.1	12.210(5)	0.4	12.228	...	12.231[d]	1
B6	$1s^22s_{1/2}2p_{3/2}3d_{5/2}$	$\frac{5}{2}$	$1s^22s_{1/2}2p_{3/2}^2$	$\frac{5}{2}$	12.142	<0.1	12.144(11)	0.1	...	...	...	...
	$1s^22s_{1/2}2p_{3/2}3d_{5/2}$	$\frac{5}{2}$	$1s^22s_{1/2}2p_{1/2}2p_{3/2}$	$\frac{5}{2}$	12.109	<0.1			...	...	...	...
B7	$1s^22s_{1/2}2p_{3/2}3d_{5/2}$	$\frac{5}{2}$	$1s^22s_{1/2}2p_{3/2}^2$	$\frac{5}{2}$	12.093	0.1	12.089(9)	0.1	...	...	12.095[e]	2
B8	$1s^22s_{1/2}2p_{3/2}3d_{3/2}$	$\frac{3}{2}$	$1s^22s_{1/2}2p_{3/2}^2$	$\frac{1}{2}$	12.083	0.1	12.038(10)	0.1	...	...	...	...
B9	$1s^22s^23d_{3/2}$	$\frac{3}{2}$	$1s^22s^22p_{3/2}$	$\frac{3}{2}$	11.948	0.2	11.977(6)	0.2	11.934	11.930	...	...
B10	$1s^22s^23d_{5/2}$	$\frac{5}{2}$	$1s^22s^22p_{3/2}$	$\frac{3}{2}$	11.934	0.1	11.932(5)	0.4	11.927	11.930	11.921	2
B11	$1s^22s_{1/2}2p_{1/2}3d_{5/2}$	$\frac{5}{2}$	$1s^22s_{1/2}2p_{1/2}2p_{3/2}$	$\frac{3}{2}$	11.885	0.1	11.881(5)	0.2	...	...	11.886	2
B12	$1s^22s_{1/2}2p_{1/2}3d_{5/2}$	$\frac{5}{2}$	$1s^22s_{1/2}2p_{1/2}2p_{3/2}$	$\frac{3}{2}$	11.799	0.1	11.802(5)	0.2	11.800	...	...	...
	$1s^22s_{1/2}2p_{3/2}3d_{3/2}$	$\frac{3}{2}$	$1s^22s_{1/2}2p^2$	$\frac{1}{2}$	11.796	<0.1		0.2	...	...	11.797	2
B13	$1s^22s^23d_{3/2}$	$\frac{3}{2}$	$1s^22s^22p_{1/2}$	$\frac{1}{2}$	11.782	1.0	11.770(3)	1	11.770	11.770	11.767	2
B14	See Table 8						11.704(11)	<0.1	...	...	11.707	1
B15	See Table 8						11.640(11)	<0.1	...	...	11.650	2
B16	See Table 8						11.578(11)	<0.1	...	...	...	...
B17	See Table 8						11.530(11)	<0.1	...	...	...	...
B18	$1s^22s_{1/2}2p_{1/2}3p_{3/2}$	$\frac{1}{2}$	$1s^22s^22p_{1/2}$	$\frac{1}{2}$	11.492	0.1	11.490(5)	0.2	11.462	...	...	...
	$1s^22s_{1/2}2p_{1/2}3p_{3/2}$	$\frac{3}{2}$	$1s^22s^22p_{1/2}$	$\frac{1}{2}$	11.505	0.1		0.2	...	...	...	...
	$1s^22s_{1/2}2p_{3/2}3p_{3/2}$	$\frac{3}{2}$	$1s^22s^22p_{3/2}$	$\frac{3}{2}$	11.509	<0.1		0.2	...	...	...	...
B19	$1s^22s_{1/2}2p_{1/2}3p_{3/2}$	$\frac{3}{2}$	$1s^22s^22p_{1/2}$	$\frac{1}{2}$	11.435	0.2	11.427(5)	0.2	11.400	...	11.440	1, 2
B20	$1s^22s_{1/2}2p_{3/2}3p_{3/2}$	$\frac{1}{2}$	$1s^22s^22p_{3/2}$	$\frac{3}{2}$	11.407	<0.1	11.400(13)	<0.05	...	...	...	

[a] Phillips et al. 1999.
[b] Mewe et al. 1985.
[c] See § 3 for explanation of relative intensity.
[d] Bromage et al. 1977 identify this line with a $J' = \frac{1}{2} \rightarrow J = \frac{3}{2}$ transition.
[e] Bromage et al. 1978 identify this line with a $J' = \frac{5}{2} \rightarrow J = \frac{5}{2}$ transition.
REFERENCES.—References from Kelly 1987 compilation: (1) Bromage et al. 1977; (2) Bromage et al. 1978.

The total measured flux in this feature is 20% of F32. This is twice the flux predicted by HULLAC.

Similar to F29, F33 consists of more than one line. The lines contributing to F33 form a broad shoulder on the high wavelength side of F34 spanning approximately 30 mÅ. We are able to fit three features into this shoulder at 11.44, 11.45, and 11.47 Å; however, because HULLAC predicts eight lines, it was not possible to assign a specific transition to any of these measured wavelengths. The measured flux relative to F34 is ≈60% which is in good agreement with the 56% that is predicted by HULLAC for all eight lines relative to F34.

The total flux of all the line emission between 11 and 12 Å in this charge state is 30% of the strongest Fe XVIII line, F20. Because this spectral region is several crystal sections away from F20, this value is only good to within a factor of 2.

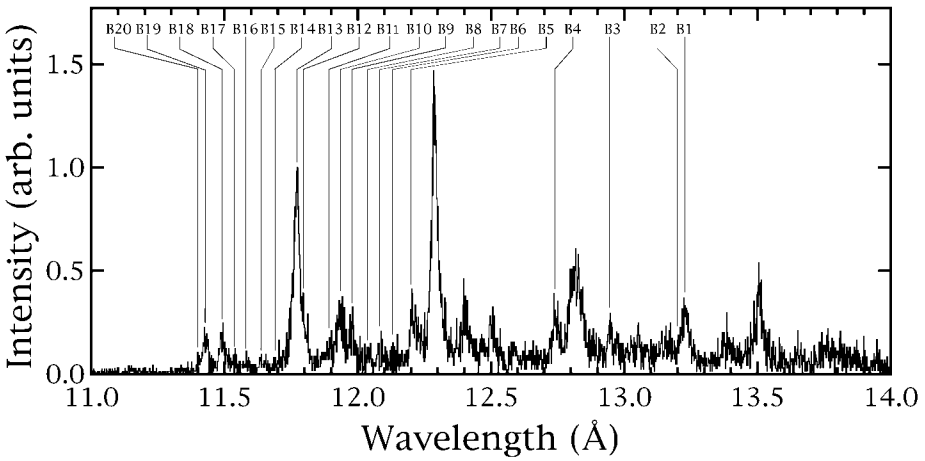

FIG. 5.—Fe XXII spectrum between 11 and 14 Å normalized to B13. The strongest line in this spectrum is C10 at 12.28 Å.

TABLE 8
LINES CONTRIBUTING TO B14–17

HULLAC λ (Å)	Upper Configuration	J'	Lower Configuration	J	Intensity[a] (%)
11.752	$1s^2 2s_{1/2} 2p_{3/2} 3d_{3/2}$	$\frac{5}{2}$	$1s^2 2s_{1/2} 2p^2_{3/2}$	$\frac{3}{2}$	2
11.746	$1s^2 2s_{1/2} 2p_{1/2} 3d_{5/2}$	$\frac{3}{2}$	$1s^2 2s_{1/2} 2p^2$	$\frac{1}{2}$	2
11.713	$1s^2 2s_{1/2} 2p_{1/2} 3p_{1/2}$	$\frac{3}{2}$	$1s^2 2s^2 2p_{3/2}$	$\frac{3}{2}$	2
11.663	$1s^2 2s_{1/2} 2p_{1/2} 3p_{3/2}$	$\frac{5}{2}$	$1s^2 2s^2 2p_{3/2}$	$\frac{5}{2}$	3
11.645[b]	$1s^2 2s_{1/2} 2p_{1/2} 3p_{3/2}$	$\frac{5}{2}$	$1s^2 2s^2 2p_{3/2}$	$\frac{3}{2}$	2
11.591[c]	$1s^2 2s_{1/2} 2p_{1/2} 3p_{1/2}$	$\frac{1}{2}$	$1s^2 2s^2 2p_{1/2}$	$\frac{1}{2}$	3
11.554	$1s^2 2s_{1/2} 2p_{1/2} 3p_{1/2}$	$\frac{3}{2}$	$1s^2 2s^2 2p_{1/2}$	$\frac{1}{2}$	2
11.534	$1s^2 2s_{1/2} 2p_{3/2} 3p_{1/2}$	$\frac{3}{2}$	$1s^2 2s^2 2p_{3/2}$	$\frac{3}{2}$	3

[a] Intensity predicted by HULLAC relative to line B13.
[b] The Fe XXII line given in the Kelly tables at 11.707 Å is also identified with this transition.
[c] The Fe XXII line given in the Kelly tables at 11.650 Å is also identified with this transition.

There are several lines in this section that are not identified as Fe XVIII. A few of these belong to Fe XVII ion, i.e., 4C (12.12 Å), 4D (12.27 Å), 3A (13.83 Å), and 3B (13.89 Å) which were measured previously (Brown et al. 1998). Four lines that are present in this spectrum and that are not from the Fe XVIII ion are at 13.71, 12.71, 12.52, and 11.38 Å. Three of these lines are background lines observed in our background spectrum and remain unidentified at this time. The line at 12.52 Å is close to the wavelength predicted to be 4F in Fe XVII; this line was not identified in the Fe XVII spectrum. We tentatively identify this line as the 4F feature.

3.2. *Oxygen-Like* Fe XIX

Oxygen-like Fe XIX has its strongest emission in the $\log T_e = 6.8$–7.0 (Arnaud & Raymond 1992) temperature range in coronal plasmas and plays a strong role in plasmas of slightly lower temperature where Fe XVII and Fe XVIII are dominant. Several authors have measured and identified Fe XIX features in solar spectra originating in both flaring and nonflaring active regions of the Sun (Phillips et al. 1982; McKenzie et al. 1980). However, it is difficult to use solar spectra to accurately measure all the Fe XIX emission contributing to this wavelength region because the Fe XIX emission is overpowered by the emission from other ions of iron. Here we present a spectrum where Fe XIX is the dominant ion, making it possible to positively identify all of its significant contributions to this wavelength band.

We have identified 34 Fe XIX features. By comparison, in the solar spectrum obtained by *SMM* and analyzed by Phillips et al. (1982), only 26 Fe XIX features were identified. In the 1999 MEKAL benchmark paper, Phillips et al. (1999) include 27 spectral features in Fe XIX above 11 Å.

3.2.1. 14.5 Å $\leq \lambda \leq$ 16.5 Å: *O1 to O13*

This wavelength section, shown in Figure 2*a*, is dominated by line emission from transitions of the type $3s \rightarrow 2p$, but includes three transitions that involve multiple photon processes, i.e., O1–O3. All of the wavelengths lines in this region are overpredicted by HULLAC by up to 60 mÅ.

The line labeled O1 has a measured wavelength that is closer to theory than any other line in this wavelength range ($\Delta\lambda = -3$ mÅ), but also has a relatively high uncertainty (± 16 mÅ). The high uncertainty is a result of the persistence of the Fe XVIII F2 feature coupled with the poor statistics in the line.

Line O4 is a blend of several features predicted to fall between 15.3 and 15.4 Å. We were able to fit two peaks to this feature, but because of the abundance of predicted lines in this region, it is not possible to assign a particular transition to any single wavelength. The average wavelength for this feature is 15.33 Å. The intensity given in Table 3 for this feature is the sum of all the flux in the region between 15.3 and 15.4 Å. The transitions that are most likely responsible for this flux and their corresponding predicted wavelengths are given in Table 3. Several features have been measured at or near these wavelengths in solar spectra that were not definitively identified. For example, Phillips et al. (1982) measured four features in the 15.29–15.43 Å range, but only tentatively identified one as Fe XVI based on a previous identification by Burkhalter et al. (1979). We do not discount this identification, but our present measurement demonstrates that there is also a contribution from the Fe XIX ion.

O5 is one of the stronger Fe XIX features. A feature near this wavelength, 15.175 Å has been identified in solar spectra as both Fe XIX and O VIII (Phillips et al. 1982). They also measure three other unidentified lines between the O VIII line at 15.17 Å and Fe XVII line 3C at 15.01 Å. The lines O6–O8 may be responsible for these features.

3.2.2. 12.5 Å $\leq \lambda \leq$ 14.5 Å: *O14 to O29*

This section consists of transitions of the type $3d \rightarrow 2p$ falling predominantly in the 13.4–13.9 Å range and the $3p \rightarrow 2s$ transitions O28 and O29. Several of the strong features in this wavelength band consist of blends. For example O14, O17, O18, O19, O20, and O21 are all blends of two or more transitions.

Lines O16 and O17 are two distinct features in our spectrum; however, HULLAC predicts five lines in this region all within 4 mÅ of one another. If the predicted spacing were correct, we would only measure a single feature because our resolving power is not high enough to separate these lines. At this time we are not able to positively assign any single predicted line to either O16 or O17.

Similar to O16 and O17, O21 is a single line feature to which we cannot assign a single predicted transition. HULLAC predicts five transitions which contribute to this line feature. The transitions are listed in Table 3.

TABLE 9
COMPARISON OF MEASUREMENTS AND CALCULATIONS OF Fe XXIII LINES

	HULLAC						THIS MEASUREMENT		PHILLIPS[a]	MEKA[b]	KELLY 1987	
LABEL	Upper	J'	Lower	J	λ (Å)	I	λ (Å)	I[c]	λ (Å)	λ (Å)	λ (Å)	Reference
Be1.....	$1s^2 2s_{1/2} 3s_{1/2}$	0	$1s^2 2s_{1/2} 2p_{3/2}$	1	12.187	0.6	12.161 (7)	0.43	12.193	12.150	...	...
Be2.....	$1s^2 2s_{1/2} 3d_{5/2}$	2	$1s^2 2s_{1/2} 2p_{3/2}$	1	11.763	1.0	11.736 (4)	1.00	11.741	11.742	11.737	1
Be3.....	$1s^2 2s_{1/2} 3s_{1/2}$	1	$1s^2 2s_{1/2} 2p_{1/2}$	1	11.730	<0.1	11.702 (5)	0.10	...	...	...	...
	$1s^2 2p_{1/2} 3d_{5/2}$	3	$1s^2 2p_{1/2} 2p_{3/2}$	2	11.715	<0.1			...	...	11.692	1, 2
Be4.....	$1s^2 2s_{1/2} 3d_{5/2}$	3	$1s^2 2s_{1/2} 2p_{3/2}$	2	11.446	0.1	11.458 (10)	0.07	11.413	11.460	11.440	3
Be5.....	$1s^2 2s_{1/2} 3d_{3/2}$	1	$1s^2 2s_{1/2} 2p_{1/2}$	1	11.344	<0.1	11.366 (10)	<0.05	...	11.360	11.333	3
Be6.....	$1s^2 2s_{1/2} 3d_{3/2}$	2	$1s^2 2s_{1/2} 2p_{1/2}$	1	11.337	0.1	11.336 (5)	0.05	...	...	11.326	1, 4
Be7.....	$1s^2 2s_{1/2} 3d_{3/2}$	1	$1s^2 2s_{1/2} 2p_{1/2}$	0	11.302	<0.1	11.285 (10)	<0.05	...	...	11.298	1
Be8.....	$1s^2 2s_{1/2} 3p_{1/2}$	1	$1s^2 2s^2$	0	11.021	0.3	11.019 (3)	0.13	...	11.020	11.018	1
Be9.....	$1s^2 2s_{1/2} 3p_{3/2}$	1	$1s^2 2s^2$	0	10.983	0.5	10.981 (3)	0.20	10.981	10.981	10.980	1

[c] See § 3 for explanation of relative intensity.
[a] Phillips et al. 1999.
[b] Mewe et al. 1985.
REFERENCES.—References from Kelly 1987 compilation: (1) Bromage et al. 1978; (2) Boiko et al. 1978; (3) Fawcett et al. 1980; (4) Bromage et al. 1977.

O24 is the strongest Fe XIX feature in our spectrum. HULLAC predicts two features near this line, one at 13.524 Å and one at 13.515 Å. The intensity of the 13.515 Å line is predicted to be 54% of that of the 13.524 Å line. We did fit a second feature, O25, at 13.497 Å which we tentatively identify as the 13.515 Å line given by HULLAC. Because of the strong influence of O24 in the fitting routine, the wavelength may be systematically shifted toward lower values.

The wavelengths of all the lines, except O22, in this wavelength band differ from those of HULLAC by ≈ -10 mÅ. This includes the $3p \rightarrow 2s$ lines at 13.02 and 12.93 Å, labeled O28 and O29, respectively.

3.2.3. 10.5 Å $\leq \lambda \leq$ 12 Å: *O30 to O34*

With the exception of one $4s \rightarrow 2p$ transition, O30, all lines measured and identified in this wavelength region (Fig. 2*c*) are of the type $4d \rightarrow 2p$. The strongest line in this region is O32 at 10.816 Å. There are four lines that are predicted to contribute to this feature, two of which are only 0.3 mÅ apart.

There are several lines contributing to the feature that is between 11.10 and 10.86 Å labeled O31. HULLAC predicts 19 lines between 11.104 and 10.838 Å responsible for O31. These lines are listed in Table 4. The combined flux of this entire feature is approximately equal to that in O32.

We are able to identify two lines at wavelengths that are lower than O32: O33 and O34. However, HULLAC predicts 27 lines in this region; four between O32 and O33, ten between O33 and O34, and 11 between O34 and the edge of the crystal bandpass, i.e., at about 10.6 Å. The complete flux between O32 and O34, including O34, is approximately 50% of O32. Because of crystal edge effects, it is not possible to reliably estimate the flux of the line emission below O34.

The region between 12.0 and 12.5 Å is not shown owing to the fact that there are no Fe XIX features contributing to this wavelength band.

There are several lines in the spectrum shown in Figure 2 which are not emitted by Fe XIX. The lines at 11.52, 11.42, and 11.32 Å are F31, F33, and F34. The lines at 13.71, 12.71, 11.38, and 15.93 Å are all background lines whose origins are unknown at this time.

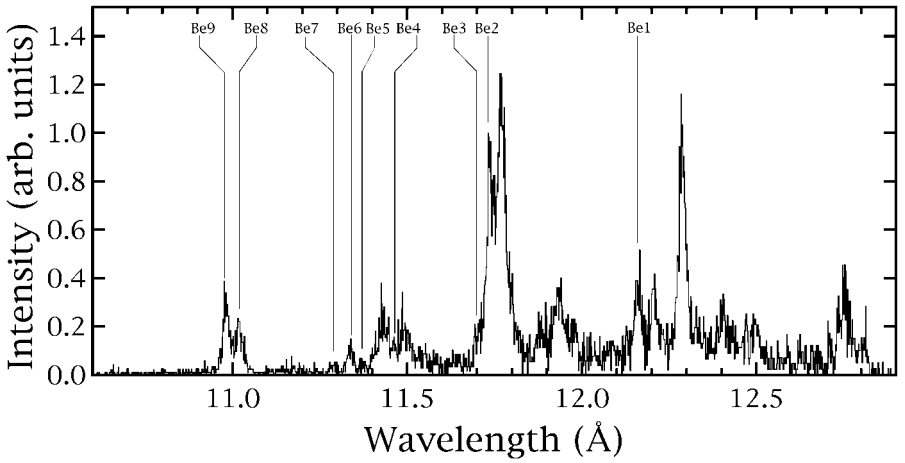

FIG. 6.—Fe XXIII spectrum between 10.6 and 12.9 Å normalized to Be2. The strongest Fe XXIII line in this spectrum is B13 at 11.77 Å.

TABLE 10

COMPARISON OF MEASUREMENTS AND CALCULATIONS OF Fe XXIV LINES

	HULLAC						THIS MEASUREMENT		PHILLIPS[a]	MEKA[b]	KELLY 1987	
LABEL	Upper	J'	Lower	J	λ (Å)	I	λ (Å)	I[c]	λ (Å)	λ (Å)	λ (Å)	Reference
Li1	$1s^2 3s_{1/2}$	$\frac{1}{2}$	$1s^2 2p_{3/2}$	$\frac{3}{2}$	11.433	0.6	11.432 (3)	0.4	...	11.445	11.426	1
Li2	$1s^2 3s_{1/2}$	$\frac{1}{2}$	$1s^2 2p_{1/2}$	$\frac{1}{2}$	11.268	0.3	11.266 (4)	0.15	...	11.269	11.261	1
Li3	$1s^2 3d_{5/2}$	$\frac{5}{2}$	$1s^2 2p_{3/2}$	$\frac{3}{2}$	11.178	1	11.176 (2)	1	11.178	11.184	11.171	1
Li4	$1s^2 3d_{3/2}$	$\frac{3}{2}$	$1s^2 2p_{1/2}$	$\frac{1}{2}$	11.034	0.6	11.029 (3)	0.6	...	11.031	11.030	1
Li5	$1s^2 3p_{1/2}$	$\frac{1}{2}$	$1s^2 2s_{1/2}$	$\frac{1}{2}$	10.663	0.5	10.663 (5)	[d]	...	10.664	10.663	1

[a] Phillips et al. 1999.
[b] Mewe et al. 1985.
[c] See § 3 for explanation of relative intensity.
[d] This intensity is unreliable because of the proximity to the edge of the crystal.
REFERENCES.—References from Kelly 1987 compilation: (1) Boiko et al. 1978.

3.3. *Nitrogen-Like* Fe xx

The Fe xx L-shell spectrum produces more lines than any other iron ion in this wavelength band. Because the Fe xx abundance peaks at log $T_e = 7$ in coronal equilibrium, its line emission is only seen in solar flares at their peak temperatures. However, larger contributions from Fe xx have been observed in higher temperature sources such as HR1099 (Brinkman et al. 2001).

3.3.1. 13.6 Å $\leq \lambda \leq$ 15.8 Å: *N1 to N14*

This wavelength section contains transitions of the type $3s \rightarrow 2p$ and several involving two photon processes whose

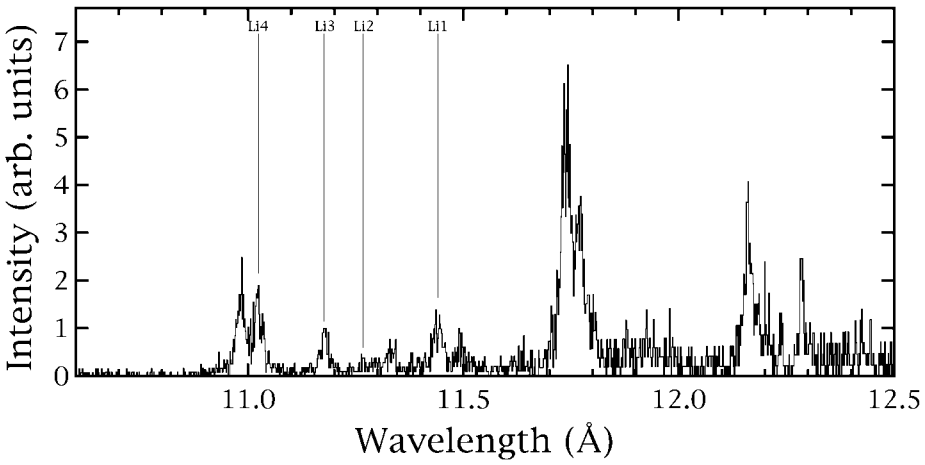

FIG. 7*a*

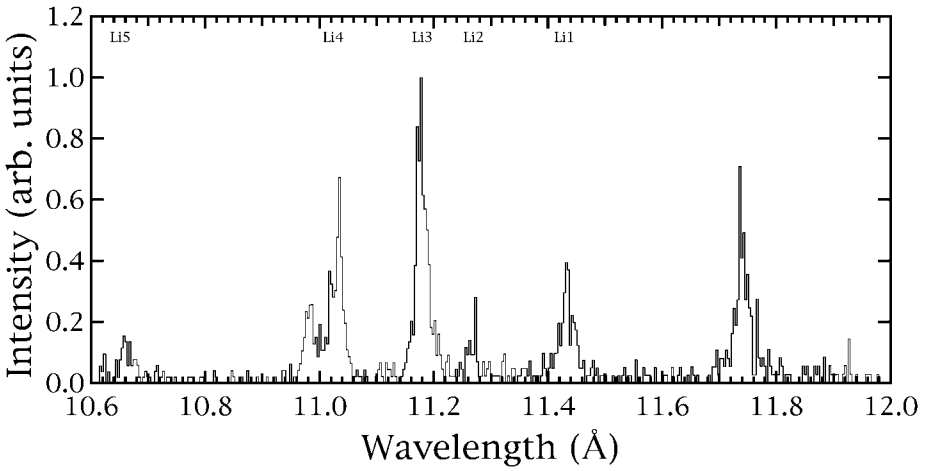

FIG. 7*b*

FIG. 7.—(*a*) Fe XXIV spectrum between 10.6 and 12.5 Å normalized to Li3 taken at a beam energy of 2 keV. (*b*) Fe XXIV spectrum between 10.6 and 12.0 Å normalized to Li3 taken at a beam energy of 4.6 keV.

upper states contain a 3*p* electron. Nearly half of the features in this wavelength region are blends of either several lines from Fe XX or lines of both Fe XX and other ion species of iron.

The Fe XX features in the vicinity of 15.0 Å effectively fill in the gaps between the diminishing Fe XIX emission. Many are only weakly indicated in the data. For example, on the short wavelength side of the weak remnant of 3C from Fe XVII at 15.01 Å, there is a sudden drop in flux at ≈14.9 Å, marking the difference between N4 and N5. We note that there is also a slight decrease in the flux at approximately 14.84 Å. This is likely the distinction between the predicted lines at 14.852 and 14.827 Å. However, a positive distinction requires better counting statistics than available in our measured spectrum. The intensity values given in Table 5 for these features include the flux from line O11 which blends with N5.

N6 contains a strong contribution from O12. A comparison of the relative intensities of N6 and O13 in the Fe XX spectrum (Fig. 3*a*) with the relative intensities of O12 and O13 in the Fe XIX spectrum (Fig. 2*a*) supports the Fe XX line identification. In the Fe XIX spectrum O13 is nearly twice as large as O12, whereas in the Fe XX spectrum the two features are approximately equal. We do note that the wavelength given for N6 is systematically shifted to a lower wavelength because of the influence of O12.

An even more "featureless" region in this section of the Fe XX spectrum is marked N8. There are three lines from Fe XX predicted to contribute to this feature. The spacing of these lines is such that they would be resolvable by our spectrometer. However, by comparing spectra from Fe XVIII and Fe XIX we find that there is still a contribution from the Fe XVIII lines F17 and F18 that "wash out" any distinct features in this region. Because the Fe XVIII features are all above 14.34 Å, and because there is no Fe XIX or Fe XXI emission predicted in this region, the section of this feature at ≈14.30 Å is likely the 14.330 Å line predicted by HULLAC.

Line N11, which is shown as a blend of two Fe XX lines, and line N12 both contain contributions from Fe XIX, O15, and O16–O17. In Figure 3*a*, the two features have roughly the same intensity, while the O16–17 feature in Figure 2*b* is much stronger than O15. Again, the difference in relative intensities allows us to assign these spectral features to the Fe XX ion. The change in intensity of the O15–N12 feature between the Fe XIX and Fe XX spectra is also accompanied by a noticeable shift of the centroid toward higher wavelength. Although it was possible to fit more than one line into this feature at both energies, the higher wavelength portion is identified as the N12 line owing to the shift in flux to the higher wavelength when going from the Fe XIX to the Fe XX charge state.

Another feature that contains flux from more than one ion species of iron is between 13.6 and 13.8 Å. Most of this feature is Fe XIX emission. The two Fe XX lines identified in this region, N13 and N14, are not present in the Fe XIX spectrum. The $1s2s\ ^3S_1 \rightarrow 1s^2\ ^1S_0$ forbidden line in Ne IX used for calibration may still contribute to this feature as it was observed in the background spectrum of this wavelength region.

3.3.2. 12.7 Å ≤ λ ≤ 13.6 Å: *N15 to N31*

This section contains all the transitions originating in a 3*d* upper level. The transitions between 13.7 and 13.0 Å do not display any systematic shift from theory; however, a comparison between measured and calculated wavelengths for the spectral features below 13 Å shows that the predicted values are approximately 10 mÅ lower than the measured values.

The line at 13.58 Å has contributions from both Fe XX and Fe XXI. It is not seen in the Fe XIX spectrum. Its centroid is measured at 13.581 Å in the Fe XX spectrum. In the Fe XXI spectrum (Fig. 4) it becomes relatively stronger and the centroid shifts to a slightly lower wavelength (13.574 Å) in the Fe XXI spectrum. There are several weak features that may contribute to this line. For Fe XX, HULLAC predicts lines at 13.565, 13.557, and 13.615 Å all to have about the same intensity (3% of the strongest Fe XX line, N31). In Fe XXI, the only feature predicted to be strong near this wavelength is at 13.618 Å. This feature is predicted to be about 3% of the strongest Fe XXI line. By noting that even the strongest Fe XXI feature does not appear in the Fe XX spectrum, we can conclude that there is no significant contribution to this feature from Fe XXI. We identify this line as an Fe XX line; however, at this time its transition can not be determined.

The feature at 13.5 Å (O24) is the strongest feature in Fe XIX and persists through the Fe XX and Fe XXI spectra. There are relatively strong lines in all three charge states near this wavelength. The feature we assign to the Fe XX charge state is predicted to have contributions from two transitions corresponding to the wavelengths 13.527 and 13.523 Å. We cannot resolve the two Fe XX features and measure their combined wavelength to be 13.535 Å (N15 in Fig. 3*b*). The measured difference between the wavelengths of N15 and O24 is 17 mÅ, which is about an order of magnitude higher than the difference of the predicted wavelength values.

The region between 13.5 and 12.8 Å contains the majority of the Fe XX line emission; however, much of it unresolved. HULLAC predicts 40 lines in this wavelength section, while we measure 11 individual line features and four large blends containing several lines each. Comparing the Fe XX spectrum in this wavelength band with Fe XIX and Fe XXI demonstrates that the emission in this region is dominated by Fe XX. We estimate the relative flux in this region to be 1.3 times the flux in N31.

The strongest Fe XX feature is N31 at 12.82 Å. Although not distinct, we were able to fit three lines into this feature. At this wavelength, HULLAC predicts three strong line features with approximately the same spacing as we measure. There are also two other much weaker Fe XX lines, 12.831 and 12.832 Å, that are predicted by HULLAC. The spectral resolution of our measurement does not allow an experimental verification of these two lines. The relative intensity of all Fe XX lines are measured relative to this entire feature, i.e., the sum of the flux of all three lines. The relative intensity of the three lines in this feature is approximately 1:2:1 for the 12.864, 12.846, and 12.824 Å lines, respectively.

3.3.3. 10.7 Å ≤ λ ≤ 12.7 Å: *N32 to N38*

The line emission in this region is comparably free from blends from other charge states and background ions. Transitions of the type $3p \rightarrow 2s$ and $3d \rightarrow 2p$ dominate this wavelength region, and there is no transition-specific systematic shift from theory observed.

Lines N36, N37, and N38 fall on top of a weak background line at 11.76 Å. Another line at 11.38 Å of comparable intensity relative to the 11.76 Å line has also been observed in the background spectrum. Since this line is not seen in the Fe XX spectrum, we conclude that there is no significant influence from the 11.76 Å background line on the Fe XX lines identified here. Other features below 11.8 Å seen in this spectrum but not marked are from Fe XVIII and Fe XIX.

3.4. *Carbon-Like* Fe XXI

The line emission from this charge state has relatively few lines in this wavelength region compared to the lower charge states of iron presented here. The transitions in Fe XXI identified in Figure 4 and Table 6 originate in a 3*p*, 3*d*, or 3*s* upper configuration. The wavelengths of all but two of the transitions are overpredicted by HULLAC by about 6 to 54 mÅ.

Similar to Fe XX, emission from Fe XXI peaks at a temperature higher than is generally seen in the Sun in places other than the hottest sections of solar flares. Lines that are routinely identified in solar spectra are C8 and C10 because they do not blend with emission from lower charge states of iron that dominate solar spectra.

As in the spectra of other charge states of iron, Fe XXI contains lines that are not resolved. C3 and C4 contribute to stronger features left over from Fe XIX and Fe XX. While the Fe XX line N15 contributes to the flux on the high-wavelength side of the N15-O24-C3 feature, Fe XXI C3 contributes to the low-wavelength side and, thus, is distinguishable from O24 and N15.

Similar to the N15-O24-C3 feature, C4 is part of a strong feature that is a blend of C4 and the three features in N31. By comparing the spectra taken at different energies where different charge states are dominant, we estimate that approximately half of this feature is from Fe XXI and that the wavelength of the Fe XXI contribution does nearly coincide with the previously mentioned Fe XX contribution to N31.

Several weak Fe XXI features are predicted between C3 and C4; owing to the weakness of these lines and the large amount of Fe XX emission still present in this spectrum we were able to ascertain that only one feature, i.e., the spectral feature at a wavelength of 12.91 Å, does not originate from Fe XX or any lower charge states. Also, we did not observe any line at this wavelength in our background spectrum. Therefore, it is reasonable to assume that this spectral feature originates from either Fe XXI or from a higher charge state of iron. However, there are no lines predicted at this wavelength neither from Fe XXI nor from any charge state to which we can assign this line.

C9 is the third blend that we identify belonging to this charge state. It creates a weak shoulder on the high-wavelength side of C10. The two lines that we identify with this blend have a combined predicted flux of 10% of C10, which agrees with our measurement.

Similar to the Fe XX ion, there are several weak features that are predicted in the wavelength range between 13.5 and 12.8 Å. HULLAC predicts 14 Fe XXI lines in this region, which we are not able to resolve. We estimate the relative flux of all the emission in this spectrum between the C4-N31 feature and the C3 feature to be 1.3 times the flux in the C4-N31 feature. Also, we estimate the total flux in the C4-N31 feature to be equal to the flux in line C10. We estimated the relative flux of these same regions in the Fe XX spectrum where no Fe XXI emission exists and found the same relative intensity. It should be noted that these values are only good to within 0.5.

3.5. B-*Like* Fe XXII

The boron-like Fe XXII spectrum presented in Figure 5 contains a large contribution from the Fe XXI ion. The measured wavelengths of the 20 Fe XXII features are given in Table 7. The strongest Fe XXII feature, B13 at 11.77 Å, is weaker than the strongest Fe XXI feature, C10 at 12.28 Å. Although there are a few strong Fe XXII features above 12.3 Å, this region is dominated by line emission from carbon-like Fe XXI.

While the region between 12.3 and 12.7 Å is dominated by Fe XXI emission, the 12.0–12.2 Å region is dominated by Fe XXII emission. We were able to fit three distinct features in this region; however, many individual lines are predicted to fall in this band. The flux contributing to this wavelength section relative to the line B13 is approximately 50%.

Similar to the region between 12.0 and 12.2 Å, the region between 11.5 and 11.7 Å contains several small features from Fe XXII. We have fitted four lines to this region with a combined flux that is 20% of the flux of B13. Because HULLAC predicts several features of similar intensity in this region we are unable to make any definite line identifications. The features predicted to contribute to this section are given in Table 8.

3.6. Be-*Like* Fe XXIII

The strong Fe XXIII feature regularly seen in high-resolution X-ray spectra (McKenzie et al. 1980; Phillips et al. 1982) is the $1s^2 2s 3d_{5/2}\ J = 2 \rightarrow 1s^2 2s 2p_{3/2}\ J = 1$ transition at 11.736 Å labeled Be2. As seen in Table 9, there are very few Fe XXIII lines identified in solar spectra.

HULLAC overpredicts all of the Fe XXIII wavelengths with the exception of Be4 and Be5. Although both of these features are very weak and, thus, the uncertainty of the measured wavelengths is relatively large, we find that the measured wavelengths are greater than the values predicted by HULLAC.

The shoulder on the low-wavelength side of Be2 consists of two weak features which blend. The combined flux of both of these features is approximately 10% of the flux of Be2.

The flux between B15 at 11.49 Å and Be3 at 11.70 Å, based on the results of HULLAC calculations, consists of several weak Fe XXII and a few Fe XXIII features. The comparison with the relative strength of distinct Fe XXII lines still present in this spectrum shows that most of the flux in this region is a result of transitions in the Fe XXII ion.

3.7. Li-*Like* Fe XXIV

The Fe XXIV spectra presented here are the simplest spectra of all the iron ions given in this wavelength range (see Figs. 7*a* and 7*b*) because there are only a few L-shell transitions which exist above 10.5 Å in Fe XXIV. This makes it relatively simple to achieve highly accurate wavelengths and intensities. Unlike the other ions of iron, we have two spectra of Fe XXIV, one at a beam energy of 2.0 keV (Fig. 7*a*) and one at 4.6 keV (Fig. 7*b*). The second, higher energy spec-

TABLE 11
AVERAGE ABSOLUTE DEVIATION FROM EBIT MEASUREMENT[a]

Ion	$\langle\lvert\lambda_{EBIT}-\lambda_{Phillips99}\rvert\rangle$	$\langle\lvert\lambda_{EBIT}-\lambda_{MEKA85}\rvert\rangle$	$\langle\lvert\lambda_{EBIT}-\lambda_{Kelly87}\rvert\rangle$
Fe XVIII	7	12	7
Fe XIX.....	11	8	9
Fe XX.....	20	13	32
Fe XXI.....	8	26	...
Fe XXII.....	16	16	10
Fe XXIII	21	16	10
Fe XXIV.....	2[b]	5	3

[a] This equals the average of the absolute value of the difference in mÅ.
[b] Phillips et al. 1999 only has one line in their list for this ion.

trum was taken in order to "burn out" most of the lower charge states. This second spectrum only spans the 10.6–11.9 Å range where the Li-like line emission exists. By comparing line strengths from other charge states of iron, such as Be2 and Be9 from Fe XXIII, it is seen that the spectrum taken at 4.6 keV is the result of a much more pure Fe XXIV charge state. Table 10 gives the summary of the Fe XXIV lines identified here.

Line Li4 may strongly blend with Be8. By comparing the wavelength of this line taken at the Fe XXIII energy (1.9 keV) with that taken at 2.0 keV and 4.6 keV, the centroid for this feature shifts from 11.019 Å to 11.022 Å between 1.9 and 2.0 keV, and then again to 11.029 Å between 2.0 and 4.6 keV. By comparing the intensities of the Fe XXIII line emission at the different energies, namely Be9 to Be8-Li4, we estimate that the contribution from Be8 to Li4 at 2.0 keV is ≈50% and at 4.6 keV is ≈10%. If it were possible to completely eliminate the Fe XXIII contribution to this feature, better agreement with the predicted wavelength may be attained.

We have identified five Fe XXIV line features in these spectra, four in both the 2.0 keV and 4.6 keV Fe XXIV spectra; and a fifth line, Li5, in the 4.6 keV spectrum. Agreement between measurement and theory is excellent with the exception of Li4 which blends with Be8. Li5 has a slightly higher uncertainty because it lies outside of the calibration lines (Ne IX Kδ at 10.764 Å is the nearest calibration line). Also, because it is close to the edge of the crystal we were unable to measure an accurate relative intensity for this line.

4. DISCUSSION AND CONCLUSION

We have presented a line survey measurement of all the significant L-shell emission from Fe XVIII–XXIV in the 10.6–17.6 Å wavelength band resulting from direct electron impact excitation from the ground state followed by radiative cascades. We have measured and identified 155 features across these seven charge states of iron, including their relative intensities. Of these 155 features, Phillips et al. (1999) include 104, Mewe et al. (1985) include 62, and Kelly (1987) includes 79. Therefore, our list is currently the most comprehensive. Table 11 gives the average absolute deviation between our measurements and Phillips et al. (1999), Mewe et al. (1985), and Kelly (1987) in mÅ. The deviations are ≈15–20 mÅ for Fe XVIII–Fe XXIII and ≈2–5 mÅ for Fe XXIV.

Combining the results given here with our previous Fe XVII measurements (Brown et al. 1998) we have measured 184 features in the 10–18 Å wavelength band. These data will provide a more complete and accurate data set that can be implemented into atomic databases to be used in the interpretation of spectra obtained by the high-resolution spectrometers aboard the *CXO*, *XMM*, and *Astro-E2* X-ray satellites. Our survey is complete in the sense that all but very weak lines produced by direct impact excitation followed by radiative cascades at an electron density near 10^{12} cm^{-3} were observed and catalogued.

Our intensity measurements are useful indicators of the relative strengths of a given line. However, this measurement was performed at only one electron energy where direct electron impact excitation plus radiative cascades are the dominant line formation processes. Processes such as resonant excitation, dielectronic excitation, or inner-shell ionization are sure to play a role in astrophysical plasmas, which contain a broad distribution of electron energies. A measurement of these excitation processes in Fe XXIV by our group showed, however, that electron-impact excitation is far the dominant line formation process under most plasma conditions (Gu et al. 1999). The same is true for Fe XXII–Fe XXIII (Gu et al. 2001). Measurements of the contribution from these processes to the spectra of lower charge states are in progress.

We are delighted to acknowledge the dedicated technical support by Dan Nelson, Ken Visbeck, Edward Magee, and Phil D'Antonio. The authors would also like to thank Vince Decaux for his help in acquiring some of the data. This work was performed at the Lawrence Livermore National Laboratory under the auspices of the US Department of Energy under Contract W-7405-Eng-48 and was supported by the NASA High Energy Astrophysics Supporting Research and Technology Program work order S-03958-G.

REFERENCES

Acton, L. W., Bruner, M. E., Brown, W. A., Fawcett, B. C., Schweizer, W., & Speer, R. J. 1985, ApJ, 291, 865
Arnaud, M., & Raymond, J. 1992, ApJ, 398, 394
Audard, M., Behar, E., Güdel, M., Raassen, A. J. J., Porquet, D., Mewe, R., Foley, C. R., & Bromage, G. E. 2001a, A&A, 365, L329
Audard, M., Güdel, M., & Mewe, R. 2001b, A&A, 365, L318
Bar-Shalom, A., Klapisch, M., & Oreg, J. 1988, Phys. Rev. A, 38, 1773
Bearden, J. 1967, Rev. Mod. Phys., 39, 78
Behar, E., Cottam, J., & Kahn, S. M. 2001, ApJ, 548, 966
Beiersdorfer, P., Brown, G. V., Chen, H., Gu, M. F., Kahn, S. M., Lepson, J. K., Savin, D. W., & Utter, S. B. 2000a, in Atomic Data Needs for X-Ray Astronomy, ed. M. A. Bautista, T. R. Kallman, & A. K. Pradhan (Greenbelt: NASA GSFC), 103
Beiersdorfer, P., et al. 2000b, Rev. Mexicana Astron. Astrofis. Ser. Conf., 9, 123
Beiersdorfer, P., & Wargelin, B. J. 1994, Rev. Sci. Instrum., 65, 13
Boiko, V. A., Faenov, A. Y., & Pikuz, S. A. 1978, J. Quant. Spectrosc. Radiat. Transfer, 19, 11

Brickhouse, N. S., Dupree, A. K., Edgar, R. J., Drake, S. A., White, N. E., Liedahl, D. A., & Singh, K. P. 1997, BAAS, 190, 2513
Brickhouse, N. S., Dupree, A. K., Edgar, R. J., Liedahl, D. A., Drake, S. A., White, N. E., & Singh, K. P. 2000, ApJ, 530, 387
Brinkman, A. C., et al. 2000, ApJ, 530, L111
———. 2001, A&A, 365, L324
Bromage, G. E., Cowan, R. D., Fawcett, B. C., Gordon, H., Hobby, M. G., Peacock, N. J., & Ridgeley, A. 1977, The Laser-produced Spectrum of Fe XVII to Fe XXI below 18 Å, Tech. Rep. CLM-R 170, Culham Laboratory, Abingdon, Oxon OX14 3DB
Bromage, G. E., Cowan, R. D., Fawcett, B. C., & Ridgeley, A. 1978, J. Opt. Soc. Am., 68, 48
Brown, G. V., et al. 2001, in Proc. 10th International Conference on the Physics of Highly Charged Ions, ed. A. Hamza & D. Schneider (Stockholm: Physica Scripta), 130
Brown, G. V., Beiersdorfer, P., Kahn, S. M., Liedahl, D. A., & Widmann, K. 1998, ApJ, 502, 1015
Brown, G. V., Beiersdorfer, P., & Widmann, K. 1999, Rev. Sci. Instrum., 70, 280
Burkhalter, P. G., Cohen, L., Cowan, R. D., & Feldman, U. 1979, J. Opt. Soc. Am., 69, 1133
Canizares, C. R., et al. 2000, ApJ, 539, L41
Cohen, L. R., & Feldman, U. 1970, ApJ, 160, L105
Cornille, M., Dubau, J., Loulergue, M., Bely-Dubau, F., & Faucher, P. 1992, A&A, 259, 669
Drake, J. J., Swartz, D. A., Beiersdorfer, P., Brown, G. V., & Kahn, S. M. 1999, ApJ, 521, 839
Fabian, A. C., Arnaud, K. A., Bautz, M. W., & Tawara, Y. 1994, ApJ, 436, L63
Fawcett, B. C., Ridgeley, A., & Ekberg, J. O. 1980, Phys. Scr., 21, 155
Feldman, U., Doschek, G. A., Cowan, R. D., & Cohen, L. 1973, J. Opt. Soc. Am., 63, 1445
Gu, M. F., Beiersdorfer, P., Brown, G. V., Kahn, S. M., Liedahl, D. A., Reed, K. J., & Savin, D. W. 2001, ApJ, 563, 462
Gu, M. F., Kahn, S. M., Savin, D. W., Behar, E., Beiersdorfer, P., Brown, G. V., Liedahl, D. A., & Reed, K. J. 1999, ApJ, 518, 1002
Kahn, S. M., Leutenegger, M. A., Cottam, J., Raun, G., Vreux, J. M., den Boggende, A. J. F., Mewe, R., & Güdel, M. 2001, A&A, 365, L312
Kastner, S. O., Bhatia, A. K., & Cohen, L. 1977, Phys. Scr., 15, 259
Kelly, R. R. 1987, J. Phys. Chem. Ref. Data, 16, 861
Klapisch, M., Schwob, J. L., Fraenkel, B. S., & Oreg, J. 1977, J. Opt. Soc. Am., 61, 148
Lepson, J. K., Beiersdorfer, P., Brown, G., Kahn, S. M., Liedahl, D. A., Mauche, C. W., Liedahl, D. A., & Utter, S. B. 2000, Rev. Mexicana Astron. Astrofis. Ser. Conf., 9, 137
Levine, M., Marrs, R., Knapp, D., & Schneider, M. 1988, Phys. Scr., T22, 157
Liedahl, D. A., Osterheld, A. L., & Goldstein, W. H. 1995, ApJ, 438, L115
Marrs, R. E. 1995, Experimental Methods in the Physical Sciences, Vol. 29A, Atomic, Molecular, and Optical Physics: Charged Particles (San Diego: Academic Press), chap. 14
Marrs, R., Beiersdorfer, P., & Schneider, D. 1994, Phys. Today, 47, 27
McKenzie, D. L., & Landecker, P. B. 1982, ApJ, 254, 309
McKenzie, D. L., Landecker, P. B., Broussard, R. M., Rugge, H. R., & Young, R. M. 1980, ApJ, 241, 409
Mewe, R., Gronenschild, E. H. B. M., & van den Oord, G. H. J. 1985, A&AS, 62, 197
Parkinson, J. H. 1973, A&A, 24, 215
Phillips, K. J. H., Leibacher, J. W., Wolfson, C. J., Parkinson, J. H., Kent, B. J., Mason, H. E., Acton, L. W., Culhane, J. L., & Gabriel, A. H. 1982, ApJ, 256, 774
Phillips, K. J. H., Mewe, R., Harra-Murnion, L. K., Kaastra, J. S., Beiersdorfer, P., Brown, G. V., & Liedahl, D. A. 1999, A&A, 138, 381
Porter, F. S., et al. 2000, in Proc. SPIE, 4140, 407
Savin, D. W., et al. 1996, ApJ, 470, L73
Wargelin, B. J., Beiersdorfer, P., Liedahl, D. A., S. M., & Goeler, S. V. 1998, ApJ, 496, 1031
White, N. E. 1996, in Cool Stars, Stellar Systems, and the Sun, ed. R. Pallavicini & A. K. Dupree (San Francisco: ASP), 193